Building an Apparatus for Ultracold Lithium-Potassium Fermi-Fermi Mixtures

MASSACHUSETTS INSTITUTE OF TECHNOLOGY
AUG 13 2010
LIBRARIES

by

Sara L. Campbell

Submitted to the Department of Physics
in partial fulfillment of the requirements for the degree of

Bachelor of Science in Physics

ARCHIVES

at the

MASSACHUSETTS INSTITUTE OF TECHNOLOGY

June 2010

© Massachusetts Institute of Technology 2010. All rights reserved.

Author .....
Department of Physics
May 21, 2010

Certified by .....
Martin W. Zwierlein
Thesis Supervisor, Department of Physics
Thesis Supervisor

Accepted by .....
David E. Pritchard
Senior Thesis Coordinator, Department of Physics

Building an Apparatus for Ultracold Lithium-Potassium Fermi-Fermi Mixtures

by

Sara L. Campbell

Submitted to the Department of Physics
on May 24, 2010, in partial fulfillment of the
requirements for the degree of
Bachelor of Science in Physics

Abstract

In this thesis, I designed and built laser systems to cool, trap and image lithium-6 and potassium-40 atoms. I also constructed the vacuum system for the experiment and experimentally tested a new method to coat the chamber with a Titanium-Zirconium-Vanadium alloy that acts as a pump. The final apparatus will use a 2D Magneto-Optical Trap (MOT) as a source of cool potassium and a Zeeman slower as a source of cool lithium. The atoms will then be trapped and cooled together in a double-species 3D MOT. In the 3D MOT, we will perform photoassociation spectroscopy on the atoms to determine the Li-K molecular energies and collisional properties. Using this information, we can transfer weakly-bound Feshbach LiK molecules into their ground state. LiK has an electric dipole moment and will open the door to the study of novel materials with very long-range interactions. This new material might form a crystal, a superfluid with anisotropic order parameter or a supersolid.

Thesis Supervisor: Martin W. Zwierlein
Title: Thesis Supervisor, Department of Physics

Acknowledgments

First, I have so much love and thanks to give to my Fermi family. I cannot imagine leaving this place that has come to feel like home. Martin always enters the lab with a loud "chyeaaa!" and dives headfirst into whatever work is to be done. The attention and care that Martin gives his students is amazing. He is one of the few people I know who would stop in the middle of running an important experiment to help me clarify something I should have learned in 8.03. Martin always made time to teach me physics, give me tons of graduate school advice, help me lock the potassium laser, and painstakingly line-edit this thesis. It was awesome to type this thesis to the sounds of Martin's late-night (early-morning!) joyful yelling from Fermi I.

From my first day, our unstoppable postdoc Peyman was kind and encouraging, with his set of phrases: "Its fiiiiiine. Don't worry! Nananana. It is amazing! I love it!" I have such fond memories of those early vacuum days when we started to put Fermi I together. When I couldn't get something to work, Peyman always helped me fix it in no time. Behind Cheng's peaceful and hardworking outer appearance I am glad to have gotten to know yardstick-wielding Sketchy Cheng, who gives us useful tips on everything from staying awake late to radiation protection in the lab. He has been a wonderful resource, as he knows the finest experimental details and can always tell you the best way to machine something.

Ibon and Peter have been my partners in Fermi II. My great friend Ibon never fails to make me laugh with his "jokes" and I love our song and dance parties in Fermi II. When I was sad Ibon said all the right things, and I felt so much better. I had a lot of fun working with Peter too, who was really awesome to stay up all night with ridiculous stat mech psets and still come into the lab, ready to work. Kevin Fischer was my UROP buddy last summer and entertained us with his stories of lost girls and grills. I have also enjoyed working with Caroline and Jacob.

The BEC I guys are also an awesome group who I wish I got to work with more! Thanks to quietly brilliant Ariel, smiling Mark, Andre the atomic physics and running up mountains beast, and our recent visitor Giacomo for their company and advice.

Ariel was really nice to do 8.422 psets with me even though I was much slower than him. BEC II, also known as AMO Walmart, deserve special thanks for repeatedly letting everyone borrow things. Dave Pritchard always stopped to chat with me in the hallway and continues to do so much for undergraduates in the department. In 8.05, Wolfgang Ketterle got me excited about cold atoms in the first place. Thanks to Joanna and Lorraine for making everything run. I also enjoyed late-night chats with our custodian Nancy, who really made me feel at home.

In the greater physics department, Javier Duarte was my partner in junior lab and life in general since the very first weeks of freshman year. We have made a great team and complemented each other very well in everything we have done. On SPS exec, Sukrit Ranjan was a wonderful leader who I could always count on in a pinch. Ed Bertschinger has put so much time and effort into the Conference for Undergraduate Women in Physics. Javier and I learned so much from Nergis Mavalvala in the second semester of junior lab. John Negele gave quantum mechanics the beauty, precision and rigor that I have always loved about math. My academic advisor Gabriella Sciolla has always given me the right advice.

This thesis could have not happened without Mark Belanger and Andrew Carvey in the Edgerton shop. I would also be nowhere without the wonderful people who trained me before I came to work for Martin, so I give tremendous credit to Al Avestruz, Steve Leeb, Joe Formaggio and Jim Spencer.

Outside of physics, Senior Haus, tEp, and the people who live there will always have a special place in my heart. Though I have disappeared for months at a time, I thank you all for welcoming me home with open arms. The unbelievably patient and reliable Dan Vickery deserves a prize for putting up with me for four years. I will really miss having him as an everyday companion. My family always put me miles before themselves. I thank my mom, dad, brother Jonathan and Julie Grandma and Fred Grandma for their every day support, countless favors, and patience with my absentmindedness. This thesis is dedicated to Fred Grandma, who I named after her cat Fred. Even in her final days, Fred Grandma was saying prayers for the lithium laser system, which just finally worked.

Contents

List of Figures

Chapter 1

Introduction

1.1 Motivation

The goal of this setup is to lay the experimental groundwork for making ultracold polar molecules of ^{6}Li and ^{40}K. Recently, the first gas of ultracold dipolar molecules in their ground state was created using ^{40}K and ^{87}Rb[26]. The dipole-dipole interactions in an ultracold dipolar gas of KRb are long-range and anisotropic, leading to physics beyond the extremely short-range Van der Waals interaction. For this particular experiment, the dipole-dipole interaction energy is only a small perturbation compared to the overall interactions, which are characterized by the Fermi energy of a few hundred nanokelvin. We assume a density of $\rho = 5 \cdot 10^{-11}$ cm^{-3}[27] so that the average radius between molecules is $r = \rho^{-1/3} \approx 24000a_0$, where a_0 is the Bohr radius. For KRb, the dipole moment is .5 Debye $= (.5 \cdot .39)ea_0$[25]. A Rydberg is a unit of energy 1 Ry $= k_e e^2/2a_0 = 13.6$ eV. Therefore, the dipole-dipole energy for KRb is,

$$E_{\text{dipole}} = k_e \frac{d^2}{r^3} = (1 \text{ Ry} \cdot 2a_0/k_e e^2) \frac{[(.5 \cdot .39)ea_0]^2}{(23800a_0)^3} = 2 \text{ Ry} \cdot \frac{(.5 \cdot .39)^2}{23800^3} \approx k_B \cdot .9\text{nK} \quad (1.1)$$

In our experiment, we hope to explore an entirely different regime of dipole-dipole interactions. The dipole moment of LiK molecules is 3.5 Debye[24], which is 7 times greater than that of KRb. The dipole-dipole interaction energy is proportional to the

square of the dipole moment, so it is 50 times greater that of KRb, or approximately $k_B \cdot 45$ nK. So in our molecular gas, electric dipole interactions will dominate and lead to exciting new phenomena such as crystal formation, superfluidity with anisotropic order parameter or supersolidity.

As in [26], we wish to transfer LiK molecules from loosely-bound Feshbach molecules to their lowest electronic, vibrational, rotational and hyperfine ground state. In [26], the authors report a procedure that is "general for bialkali polar molecules." The procedure requires knowledge of the energy levels of the molecules. On our new apparatus, we will perform photoassociation spectrocopy to characterize the LiK energy levels and find transitions suitable for the formation of ground state molecules.

1.2 Overview of Experiment

Our experiment will have a 2D Magneto-Optical Trap (MOT) as a source of cold $^{40\prime}$K atoms and a Zeeman slower as a source of cold ^{6}Li atoms. The atoms will be trapped together in a double-species 3D MOT. For photoassociation spectroscopy, we only need to cool the atoms to MOT temperatures and we only need a vacuum of 10^{-8} Torr. However, using our new Titanium-Zirconium-Vanadium pump coating technique we hope to get pressures of 10^{-10} Torr or better that are suitable for degenerate quantum gases. We need potassium and lithium laser systems for cooling, trapping, controlling and imaging the atoms. To stabilize the laser frequency, we lock master lasers to the frequency of an atomic resonance and then shift the master laser frequency as necessary. Once we have cold lithium and potassium atoms in the MOT, we will perform photoassociation spectroscopy. To do photoassociation spectroscopy, we shine a laser at the atoms and sweep the frequency. At certain frequencies, the laser will pump the atoms into different molecular states. The formation of molecules will change the atom number in our MOT. By looking at the features of graph of atom number vs. laser frequency, we will be able to determine the molecular energy levels.

1.3 Thesis Overview

Chapter 2 derives the light scattering force and absorption and dispersion of a laser beam by a cloud of atoms classically. The we discuss basic methods of cooling and trapping neutral atoms: Zeeman slowers, optical molasses and magneto-optical traps.

Chapter 3 describes the lithium and potassium laser systems. We discuss saturated-absorption spectroscopy that shows us atomic lines and frequency-modulation spectroscopy that we use to generate an error signal for locking the laser frequency. Then we describe how we use feedback to lock the laser, double-pass acousto-optical modulators (AOMs) to get different laser frequencies. We review Fabry-Perot interferometers, because we will soon build one for lithium and one for potassium to check that we have the right frequencies. The section ends by reviewing some recent updates to our homemade laser designs.

Chapter 4 describes our vacuum system for the 2D MOT/Zeeman slower/3D MOT apparatus.

Chapter 5 concludes the thesis by discussing the work to be completed in the near future and also by suggesting some improvements to our current apparatus designs.

Chapter 2

Theory

2.1 Lorentz Model

2.1.1 Frequency Response of a Single Atom

We want to understand qualitatively what happens when an atom with a single outer electron interacts with coherent, monochromatic light. We model the atom as an electron on a spring with damping, in the presence of an external field $E(x,t)$. Let x be the position of the electron and ω_0 be the natural frequency of the oscillator. Then, assuming nonrelativistic speeds, the Lorentz force is $F = eE$ and the restoring force is $F = -m\omega_0^2 x$, so[3],

$$\ddot{x} + 2\gamma\dot{x} + \omega_0^2 x = \frac{e}{m}E. \tag{2.1}$$

The general solution to this differential equation is the sum of the solution to the associated homogeneous differential equation, which will give us the transient behavior and any particular solution, which will give us the steady state behavior. Let $E = E_0 e^{i\omega t}$, and let us consider the steady state behavior where the electron oscillates with an amplitude x_0 at the same frequency ω, but lagging behind the drive by

a phase shift ϕ, so that $x = x_0 e^{i\phi} e^{i\omega t}$. Plugging this into equation (2.1) gives,

$$x_0 e^{i\phi}(-\omega^2 + i2\gamma\omega + \omega_0^2) = \frac{eE_0}{m} e^{i\omega t}, \tag{2.2}$$

so,

$$x_0 e^{i\phi} = \frac{1}{(\omega_0^2 - \omega^2) + i(2\gamma\omega)} \frac{e}{m} E_0 e^{i\omega t}. \tag{2.3}$$

Solving for the amplitude and phase of the steady state response, we find,

$$x_0 = \frac{eE_0/m}{\sqrt{(\omega_0^2 - \omega^2)^2 + (2\gamma\omega)^2}}, \tag{2.4}$$

and,

$$\phi = \tan^{-1}\left(\frac{2\gamma\omega}{\omega_0^2 - \omega^2}\right). \tag{2.5}$$

In figure 2-1, the amplitude and phase are plotted as a function of frequency. The normalized amplitude $x_0/(eE_0/m\omega_0^2)$ is 1 for a static field E_0 where we simply find the displacement $eE_0/m\omega_0^2$ by a balance of static forces. The normalized amplitude is 0 for large frequencies because the drive oscillates too quickly for the system to respond efficiently. There is a resonance peak $\omega = \omega_0$, which is very high for a small linewidth ($\propto \gamma$). As shown in figure 2-1 The phase ϕ is 0 for small frequencies, $-\pi/2$ at resonance, and $-\pi$ at large frequencies.

2.1.2 Index of Refraction of a Gas

From our analysis of the frequency response of a single atom, we can find the index of refraction of a gas with N atoms per unit volume, all oscillating with natural frequency ω_0. The electric dipole moment per unit volume is,

$$P = -Nex. \tag{2.6}$$

Let ϵ be the permittivity of the gas and ϵ_0 be the permittivity of free space. Let $\kappa_e = \epsilon/\epsilon_0 = 1 + \chi_e$ be the relative permittivity of the gas, where χ_e is the electric susceptibility of the gas. Let n be the index of refraction, which is related to the

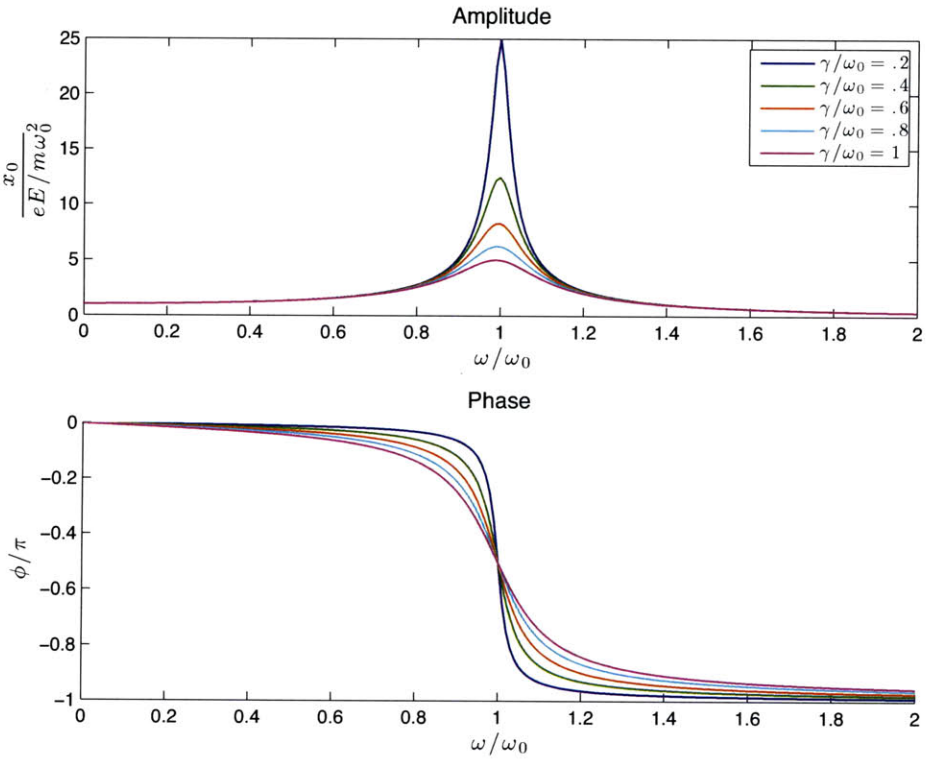

Figure 2-1: The normalized amplitude $\frac{x_0}{eE_0/m\omega_0^2}$ and phase ϕ/π plotted as a function of normalized frequency ω/ω_0 for different values of the normalized damping factor γ/ω_0.

relative permittivity by $n^2 = \kappa_e$. All of the above parameters of the gas can have both real and complex parts. As we will show, the complex parts describe losses in an electromagnetic wave as it propagates through the medium. The electric dipole moment per unit volume P is directly proportional to E,

$$P = \chi_e E = \epsilon_0(\kappa_e - 1)E, \tag{2.7}$$

so,

$$\kappa_e = 1 + \frac{P}{\epsilon E} \tag{2.8}$$

To find P/E, we plug our expression for x, equation (2.3) in the previous section, into equation (2.6) and find,

$$P = \left[\frac{Ne^2/m}{w_0^2 - \omega^2 + i2\gamma\omega}\right] E. \tag{2.9}$$

Therefore,

$$n^2 = \kappa_e = 1 + \frac{Ne^2/m\epsilon_0}{(\omega_0^2 - \omega^2) + i(2\gamma\omega)} = 1 + \frac{Ne^2/m\epsilon_0\left[(\omega_0^2 - \omega^2) - i(2\gamma\omega)\right]}{(\omega_0 - \omega^2)^2 + (2\gamma\omega)^2}. \tag{2.10}$$

Let $n = n_r - in_i$ and $k = k_r - ik_i$. They are related in the usual way,

$$n = n_r - in_i = kc/\omega = (c/\omega)(k_r - ik_i). \tag{2.11}$$

To understand what a complex index of refraction and a complex wavenumber mean, we consider what happens when the traveling wave $E = E_0 e^{i(\omega t - kz)}$ propagates in a medium with the above k and n,

$$E_0 e^{-(\omega n_i/c)z} e^{i(\omega t - \omega n_r/c)z}. \tag{2.12}$$

Therefore, the amplitude of the wave decays exponentially, with decay constant proportional to the complex component of the index of refraction. The absorption coefficient α is defined so that the light intensity ($\propto E^2$) drops to $1/e$ after it travels a

distance $1/\alpha$,

$$\alpha = \frac{2\omega n_i}{c}. \tag{2.13}$$

To finish the story, we solve for n_r and n_i. For a gas, κ_e is usually approximately 1, so we can Taylor expand the expression for n,

$$n = \sqrt{\kappa_e} = \sqrt{1 + (\kappa_e - 1)} \approx 1 + \frac{1}{2}(\kappa_e - 1). \tag{2.14}$$

Therefore,

$$n_r = \frac{\kappa_r + 1}{2} = 1 + \frac{Ne^2}{2m\epsilon_0} \frac{\omega_0^2 - \omega^2}{(\omega_0^2 - \omega^2)^2 + (2\gamma\omega)^2} \tag{2.15}$$

$$n_i = \frac{\kappa_i}{2} = \frac{Ne^2}{2m\epsilon_0} \frac{2\gamma\omega}{(\omega_0^2 - \omega^2)^2 + (2\gamma\omega)^2}. \tag{2.16}$$

In figure 2-2, we plot the real and complex components of the index of refraction, normalized in the following way,

$$\frac{2m\epsilon_0}{Ne^2 w_0^2}(n_r - 1) = \frac{1 - (\frac{\omega}{\omega_0})^2}{(1 - (\frac{\omega}{\omega_0})^2)^2 + (2\frac{\gamma}{\omega_0}\frac{\omega}{\omega_0})^2} \tag{2.17}$$

$$\frac{2m\epsilon_0}{Ne^2 w_0^2}(n_i) = \frac{2\frac{\gamma}{\omega_0}\frac{\omega}{\omega_0}}{(1 - (\frac{\omega}{\omega_0})^2)^2 + (2\frac{\gamma}{\omega_0}\frac{\omega}{\omega_0})^2} \tag{2.18}$$

for different values of the normalized damping coefficient γ/ω_0.

2.2 Spontaneous Light Force

The 1997 Nobel Prize in Physics was given to Steven Chu, Claude Cohen-Tannoudji and William Phillips, "for development of methods to cool and trap atoms with laser light."[2] When an atom absorbs a photon with energy $E = \hbar\omega$ and momentum $p = \hbar\vec{k}_{\text{abs}}$, the atom recoils. When the atom emits a photon, it recoils again $\hbar\vec{k}_{\text{emit}}$. Atoms spontaneously emit photons randomly in all directions, so the average recoil due to the spontaneously emitted photons is zero. Therefore, assuming only spontaneous emission of photons, the net force on the atom is just due to the photons that it

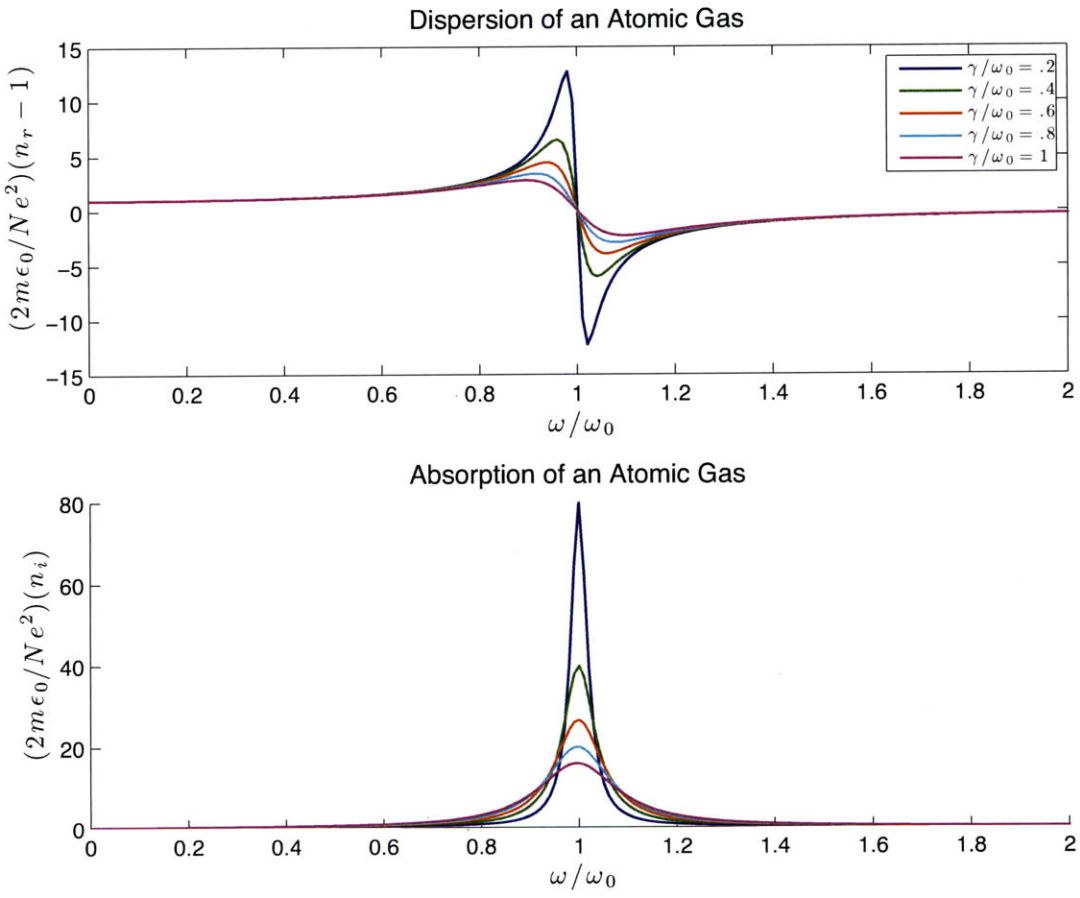

Figure 2-2: Normalized dispersion and absorption curves for an atomic gas.

absorbs.

We consider a two-level atom with ground state $|g\rangle$ and excited state $|e\rangle$ in an electromagnetic field with electric field operator,

$$\vec{\epsilon}(\vec{r,t}) = \vec{E_0}\cos(kz - \omega_l t) \tag{2.19}$$

The Rabi frequency is defined to give the strength of the electric dipole coupling between the ground and excited states in the presence of the electric field[22],

$$\hbar\Omega \equiv -eE_0\langle e|r|g\rangle \tag{2.20}$$

We define the saturation intensity I_0 as the intensity of light at which the Rabi frequency becomes $\Omega = \Gamma/\sqrt{2}$[19] so that,

$$\frac{I}{I_0} = \frac{2\Omega^2}{\Gamma^2} \tag{2.21}$$

The photon scattering rate looks similar to our classical Lorentzian frequency response derived earlier and is,

$$\gamma_s = \frac{\Gamma}{2}\frac{I/I_0}{1 + I/I_0 + (2\delta/\Gamma)^2}, \tag{2.22}$$

where δ is the detuning of the laser from the atomic resonance. The average net force of a laser beam of photons on an atom is the average change in momentum of the atom over time, which is given by the product of the recoil momentum $\hbar k$ and the average scattering rate[19][22],

$$\vec{F} = \hbar\vec{k}\frac{\Gamma}{2}\frac{I/I_0}{1 + I/I_0 + (2\delta/\Gamma)^2} \tag{2.23}$$

The maximum possible force occurs when there is infinite laser power so that the atoms spend half of their time in the ground state and half of their time in the excited state,

$$F_{\max} = \frac{\hbar k\Gamma}{2}. \tag{2.24}$$

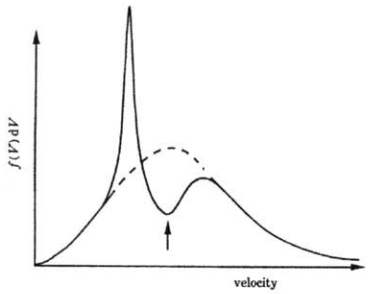

Figure 2-3: Theoretical velocity distribution after atoms with an initial velocity distribution shown by the dashed line are slowed down by a laser with fixed frequency indicated by the arrow. From William Phillips' Varenna Lecture [28].

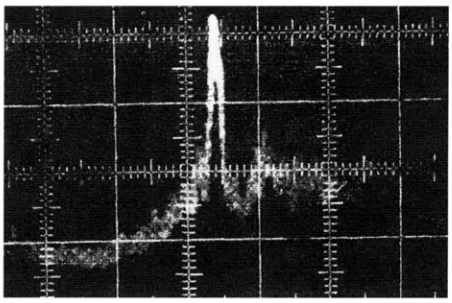

Figure 2-4: Atom fluorescence vs. probe laser frequency data from the first observation of the cooling of an atomic beam as reported in [5].

2.3 Zeeman Slower

As shown in figures 2-3 and 2-4 light of a fixed laser frequency only interacts with a small portion of the total velocity distribution. One solution to cool down a larger portion of the velocity distribution is chirp cooling, where the frequency of the counterpropagating laser is swept using electro-optical modulators to address a wide range of velocity classes[13]. The solution we discuss here is the Zeeman slower, where the counterpropagating laser frequency remains fixed, but the energy spacing of the ground and excited states of the atom, and thus the resonance frequency, is Zeeman shifted in space. The capture velocity v_c is the highest velocity atom that can be slowed to nearly zero velocity. The particular Zeeman slower we are using for lithium is a spin-flip Zeeman slower originally designed for sodium and described in Ananth Chikkatur's Ph.D. thesis[11].

2.4 Choosing the Length

The atoms moving at the capture velocity v_c are slowed down for the entire length of the slower,

$$\frac{1}{2}mv_c^2 = mfa_{\max}L, \tag{2.25}$$

where,

$$a_{\max} = \frac{\hbar k \Gamma}{2m} \tag{2.26}$$

is the maximum acceleration as in equation (2.24) and f is the fraction of the maximum acceleration we can achieve with our finite intensity laser[11]. Therefore,

$$v_c = \sqrt{2 f a_{\max} L} \tag{2.27}$$

Our goal in designing a Zeeman slower is to maximize the flux of cold atoms that make it to the magneto-optical trap. The atomic beam comes out of a nozzle that only allows a small solid angle of velocity directions through. The beam of atoms expands ballistically in the transverse direction so that flux of atoms at te end of the slower Φ decreases with the length L of the slower,

$$\Phi = \frac{\Phi_0}{L^2}. \tag{2.28}$$

The speed of the atoms follows the Maxwell-Boltzmann distribution[29],

$$N(v) = N\sqrt{\frac{2}{\pi}\left(\frac{m}{kT}\right)^3} v^2 e^{\frac{-mv^2}{2kT}}, \tag{2.29}$$

so $N(v) \propto v^2$ for small v, and $\Phi(v) \propto v \cdot N(v)$, so $\Phi(v < v_c) = \int_0^{v_c} v^3 dv = v_c^4$. Combining the effects of transverse expansion and capture velocity we have,

$$\Phi \propto \frac{v_c^4}{L^2} \propto \frac{(\sqrt{L})^4}{L^2} = \frac{L^2}{L^2}. \tag{2.30}$$

Therefore, to the first order, the flux of atoms does not depend on the length of the Zeeman slower! At larger velocities, the Maxwell-Boltzmann distribution rolls over as the $e^{\frac{-mv^2}{2kT}}$ term starts to have an effect. This tells you to make the Zeeman slower shorter because the gains from capturing more atoms no longer compete with the transverse spreading. Another reason to keep the length short is transverse heating due to the slower beam. The higher-velocity atoms must absorb and emit many photons to be slowed down. The atoms absorb photons from one direction, but

spontaneously emit photons in a random direction, leading to transverse heating. At the end of the slower, transverse velocities approach longitudinal velocities, leading to "blowing" of the beam. However, a longer slower can act as a better differential pump between the nozzle and the main chamber, which will give a better pressure in the main chamber and thus a greater atom number in the final 3D MOT.

2.5 Magnetic Field Profile

Let δ_0 be the detuning of a laser beam from the frequency of an atomic transition for an atom at rest with no external fields and let $\vec{k}$ be the wavenumber of the laser beam wave. Then the, for a cycling transition between two stretched states, the detuning δ for an atom moving at velocity v in the presence of a spatially-varying magnetic field $B(z)$ is[15],

$$\delta = \delta_0 - \vec{k} \cdot \vec{v} \pm \frac{\mu_B}{\hbar} B(z), \tag{2.31}$$

where μ_B is the Bohr magneton and the sign of the Zeeman shift depends on which transition and therefore which polarization of light we are using. We plug in the velocity,

$$v = \sqrt{v_c^2 - 2 f a_{\max} z} \tag{2.32}$$

and set the detuning δ to be zero so that the light is always on resonance with the atomic beam. Now we can solve for the magnetic field,

$$B(z) = \frac{\delta_0 \hbar}{\mu_B} \pm \frac{\hbar k v_c}{\mu_B} \sqrt{1 - \frac{2 f a_{\max} z}{v_c^2}} \tag{2.33}$$

This particular slower was designed to have a capture velocity for sodium of 950 m/s. The first 75 cm of the slower are designed for $f = .6$ and the later centimeters are designed for $f = .4$.

2.6 1D Optical Molasses

The following derivation follows the one in [28] and fills in some more steps. Here we consider an atom moving at velocity v between two counterpropagating laser beams detuned from the atomic transition frequency by δ. An atom moving at velocity v sees light with frequency ν_0 in the lab frame Doppler-shifted by,

$$\Delta\nu = -\nu_0\frac{v}{c} = -\frac{c}{\lambda_0}\frac{v}{c} = -kv, \tag{2.34}$$

in the frame moving with the atom. So to find the force that the atom feels, we sum the light force for the laser beams moving to the right and left, replacing δ in equation (2.23) by $(\delta - kv)$. In the limit where the intensity of the beam is small $I \ll I_0$,

$$F = F_{\text{right}} - F_{\text{left}} = \hbar k\frac{\Gamma}{2}\frac{I/I_0}{1+\left[\frac{2(\delta-kv)}{\Gamma}\right]^2} - \hbar k\frac{\Gamma}{2}\frac{I/I_0}{1+\left[\frac{2(\delta+kv)}{\Gamma}\right]^2}. \tag{2.35}$$

F vs. v is plotted for various values of the detuning δ in figure 2-5. The force is maximized around when $\delta = \Gamma/2$.

The force looks linear for small v. To show this, we expand equation (2.35),

$$F = \hbar k\frac{\Gamma}{2}\frac{I}{I_0}\left[\frac{1}{1+\frac{2\delta^2}{\Gamma}-\frac{4\delta kv}{\Gamma}+\left(\frac{2kv}{\Gamma}\right)^2} - \frac{1}{1+\frac{2\delta^2}{\Gamma}+\frac{4\delta kv}{\Gamma}+\left(\frac{2kv}{\Gamma}\right)^2}\right]. \tag{2.36}$$

We assumed small v so,

$$\left(\frac{2kv}{\Gamma}\right)^2 \approx 0. \tag{2.37}$$

Now we add the two fractions,

$$F = \hbar k\frac{\Gamma}{2}\frac{I}{I_0}\left[\left(\frac{1}{1+\frac{2\delta^2}{\Gamma}-\frac{4\delta kv}{\Gamma}}\right)\left(\frac{1+\frac{2\delta^2}{\Gamma}+\frac{4\delta kv}{\Gamma}}{1+\frac{2\delta^2}{\Gamma}+\frac{4\delta kv}{\Gamma}}\right) - \left(\frac{1}{1+\frac{2\delta^2}{\Gamma}+\frac{4\delta kv}{\Gamma}}\right)\left(\frac{1+\frac{2\delta^2}{\Gamma}-\frac{4\delta kv}{\Gamma}}{1+\frac{2\delta^2}{\Gamma}-\frac{4\delta kv}{\Gamma}}\right)\right] \tag{2.38}$$

$$= \hbar k\frac{\Gamma}{2}\frac{I}{I_0}\left[\frac{\frac{8\delta kv}{\Gamma}}{\left(1+\frac{2\delta^2}{\Gamma}\right)^2-\left(\frac{4\delta kv}{\Gamma}\right)^2}\right] \approx 2\hbar k^2\frac{\left(\frac{2I}{I_0}\right)\left(\frac{2\delta}{\Gamma}\right)}{\left[1+\left(\frac{2\delta}{\Gamma}\right)^2\right]^2}v, \tag{2.39}$$

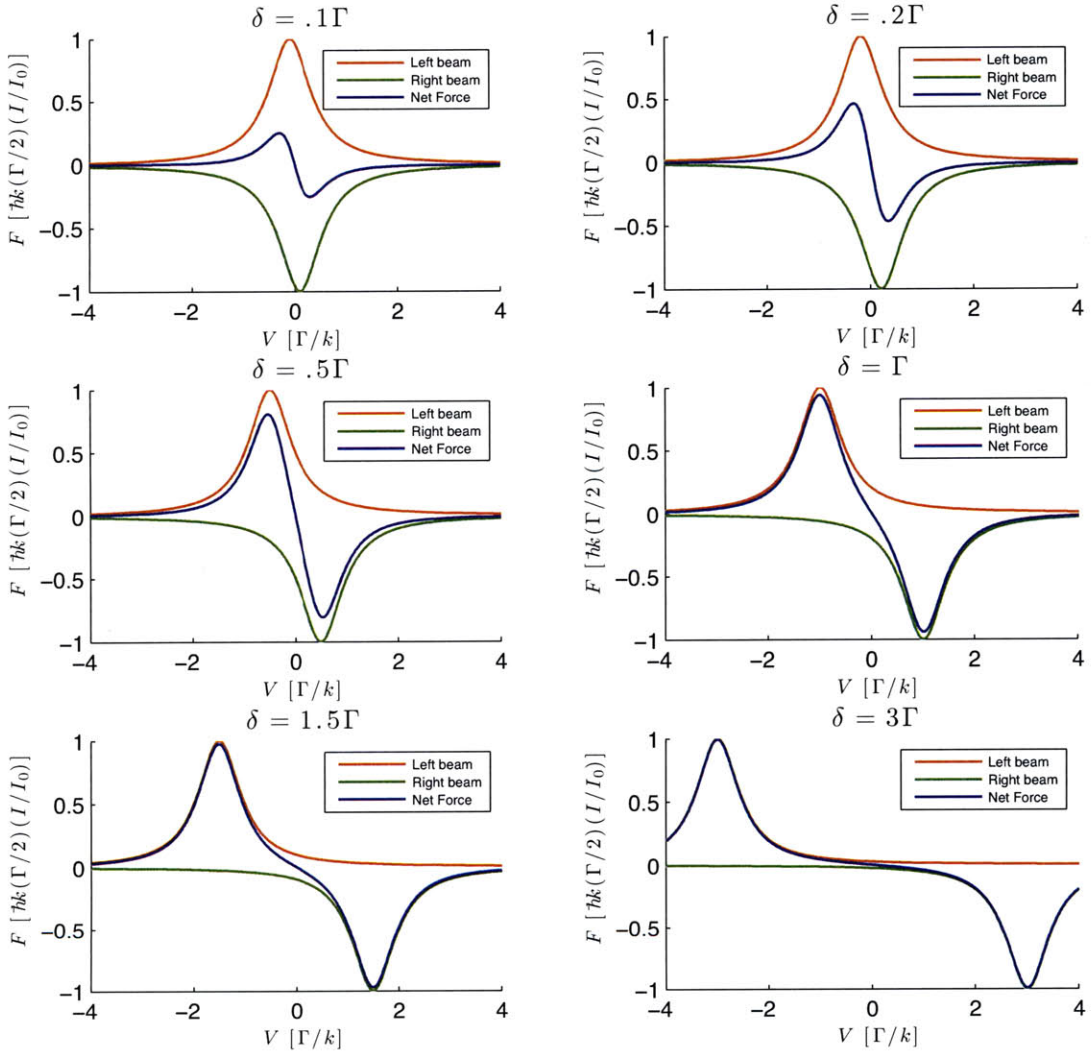

Figure 2-5: Optical molasses force plotted for various values of the detuning δ. Inspired by [28].

where we again use the fact that v is small. If the laser is red-detuned, that is if $\delta < 0$, then the atom experiences a damping force $F = -\alpha v$. This means that as long as the atoms are initially moving with a small enough velocity so that the force $F(v)$ is in the linear regime, the atoms are captured by the molasses, and slowed down to the Doppler cooling limit where there is randomness in the motion caused by the spontaneously emitted photons.

2.6.1 1D Magneto-Optical Trap

The power series expansion of the magnetic field from a current loop of radius R and current I at distance D from the origin is, in cylindrical coordinates[23],

$$B_z = \mu I \frac{1}{2} \frac{R^2}{(D^2+R^2)^{(3/2)}} + \mu I \frac{3}{2} \frac{DR^2}{(D^2+R^2)^{(5/2)}} z + \cdots \tag{2.40}$$

$$B_\rho = -\mu I \frac{3}{4} \frac{DR^2}{(D^2+R^2)^{(5/2)}} \rho. \tag{2.41}$$

If we place two loops in the anti-Helmholtz configuration as shown in figure 2-6, then the odd terms in equations (2.40) and (2.41) sum constructively and we get,

$$B_z = \mu I \frac{R^2}{(D^2+R^2)^{(3/2)}} + \mu I \frac{3}{2} \frac{DR^2}{(D^2+R^2)^{(5/2)}} z + \cdots \tag{2.42}$$

$$B_\rho = -\mu I \frac{3}{2} \frac{DR^2}{(D^2+R^2)^{(5/2)}} \rho. \tag{2.43}$$

For $2D = R$, the gradient is maximized [23],

$$\frac{dB_z}{dz} = 2\frac{dB_\rho}{d\rho} = \mu I \frac{48}{25\sqrt{5}R^2}. \tag{2.44}$$

Substituting $\delta + kv + \beta z$ for $\delta + kv$ in equation (2.35) we have,

$$F = F_{\sigma^+} - F_{\sigma^-} = \hbar k \frac{\Gamma}{2} \frac{I/I_0}{1 + \left[\frac{2(\delta - kv - \beta z)}{\Gamma}\right]^2} - \hbar k \frac{\Gamma}{2} \frac{I/I_0}{1 + \left[\frac{2(\delta + kv + \beta z)}{\Gamma}\right]^2}. \tag{2.45}$$

And using the same procedure as for optical molasses, in the limit of small velocity

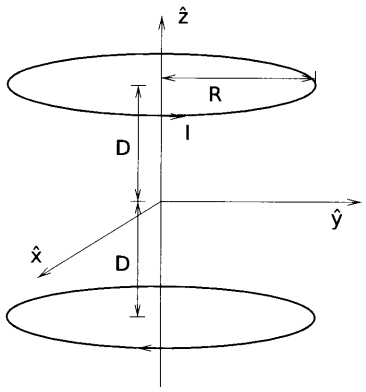

Figure 2-6: Illustration of two current loops in the anti-Helmholtz configuration. Image from [23].

v and Zeeman-shift β, we find that the force is approximately linear in $(kv + \beta z)$,

$$F \approx 2\hbar k \frac{\left(\frac{2I}{I_0}\right)\left(\frac{2\delta}{\Gamma}\right)}{\left[1+\left(\frac{2\delta}{\Gamma}\right)^2\right]^2}(kv + \beta z). \tag{2.46}$$

Let the atoms have mass M. Then,

$$F = Mz'' = 2\hbar k \frac{\left(\frac{2I}{I_0}\right)\left(\frac{2\delta}{\Gamma}\right)}{\left[1+\left(\frac{2\delta}{\Gamma}\right)^2\right]^2}(kz' + \beta z). \tag{2.47}$$

For negative detuning, we see that the atoms in the trap behave like a damped harmonic oscillator,

$$z'' + \gamma z' + \omega_{\text{trap}}^2 = 0, \tag{2.48}$$

where,

$$\gamma = -\frac{4\hbar k^2 \left(\frac{I}{I_0}\right)\left(\frac{2\delta}{\Gamma}\right)}{M\left[1+\left(\frac{2\delta}{\Gamma}\right)^2\right]^2}, \tag{2.49}$$

and,

$$\omega_{\text{trap}}^2 = -\frac{4\hbar k \left(\frac{I}{I_0}\right)\beta\left(\frac{2\delta}{\Gamma}\right)}{M\left[1+\left(\frac{2\delta}{\Gamma}\right)^2\right]^2}. \tag{2.50}$$

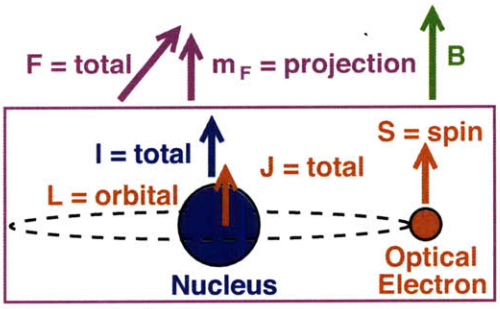

Figure 2-7: Overview of the relevant quantum numbers for our atoms.

So, both the velocity and the position of the atoms in a MOT ring down.

2.7 Our Atoms

We refer to the states of our atoms using spectroscopic notation,

$$N^{2S+1}L_J, \tag{2.51}$$

where N is the often-omitted principal quantum number, S is the total spin number and $(2S+1)$ is the number of spin states, L refers to the principal quantum number $l = 0, 1, 2, 3, \ldots$ written as $S, P, D, F, \ldots$ and J is the total electron angular momentum quantum number. $F = J + S$ is the total spin quantum number, and we label our hyperfine states by their F values. An overview of all of these quantum numbers and what they mean is shown in figure 2-7. The stretched states where all of the angular momentum of the electron and the nucleus are aligned[35] and

$$|m_F| = F = I + J = I + L + S \tag{2.52}$$

We cool on a closed cycling transition between the ground and the excited stretched state with circularly polarized σ_+ light These states are also nice to deal with when we want to Zeeman shift them, because the magnetic moment is a constant function of an external applied magnetic field B, so they are just straight lines in a Breit-Rabi

diagram, separated in energy by $\mu_B B$ where μ_B is the Bohr magneton.

2.7.1 Lithium

We can write the hyperfine energy levels in terms of the magnetic dipole constant A and the electric quadrupole constant B as[6],

$$W_F = \frac{1}{2}hAK + hB\frac{\frac{3}{2}K(K+1) - 2I(I+1)J(J+1)}{2I(2I-1)2J(2J-1)}, \tag{2.53}$$

where $K = F(F+1) - I(I+1) - J(J+1)$. The hyperfine splitting at the $2^2S_{1/2}$ level is 228 MHz and the hyperfine coupling constant A at that level is $\approx$ 17.5 MHz.[6] To determine where the hyperfine energies lie with respect to the $2^2S_{1/2}$ level, we compute,

$$K_{F=1/2} = \frac{1}{2}\cdot\frac{3}{2} - 1\cdot 2 - \frac{1}{2}\cdot\frac{3}{2} = -2 \tag{2.54}$$

$$K_{F=3/2} = \frac{3}{2}\cdot\frac{5}{2} - 1\cdot 2 - \frac{1}{2}\cdot\frac{3}{2} = 1 \tag{2.55}$$

Therefore $2^2S_{1/2}$ is at -152 MHz and $2^2S_{1/2}$ is at 76 MHz with respect to the $2^2S_{1/2}$ fine splitting level. $A \approx 17.5$ MHz for $2^2P_{1/2}$ and $A \approx -1.16$ MHz for $2^2P_{3/2}$[6][20], so we compute the hyperfine splittings $\frac{1}{2}A\Delta K$ and the positions with respect to the fine splittings similarly, double-checking with [20]. The energy level diagram for lithium is shown in figure 2-8.

2.7.2 Potassium

The energy level diagram for potassium can be explained in a similar way and is shown in figure 2-9. In contrast to lithium, we lock the master potassium laser to a commercial vapor cell with mostly ^{39}K inside and then shift from that starting frequency to cool and trap ^{40}K.

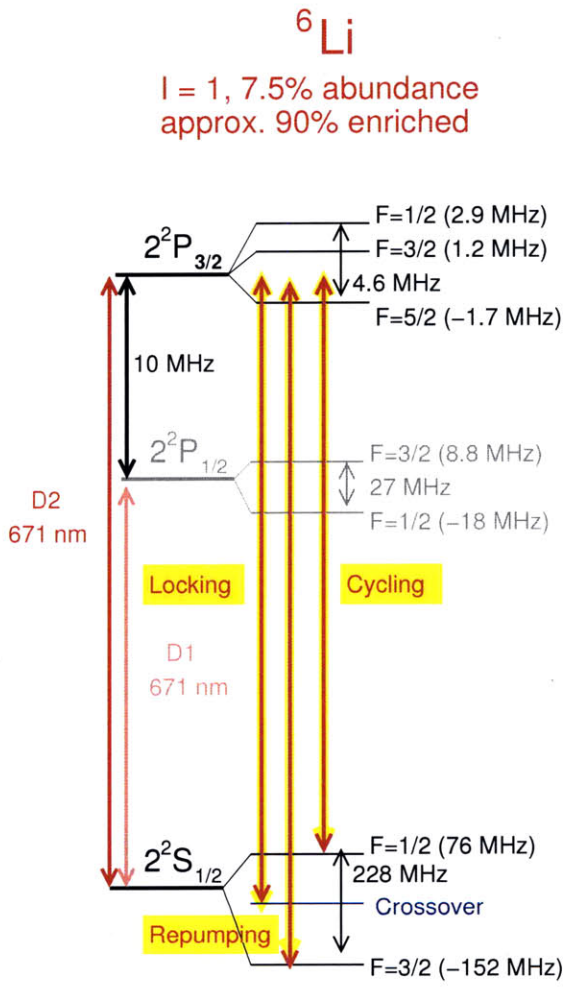

Figure 2-8: Hyperfine structure and relevant transitions for ^{6}Li that we lock to, cool and control.

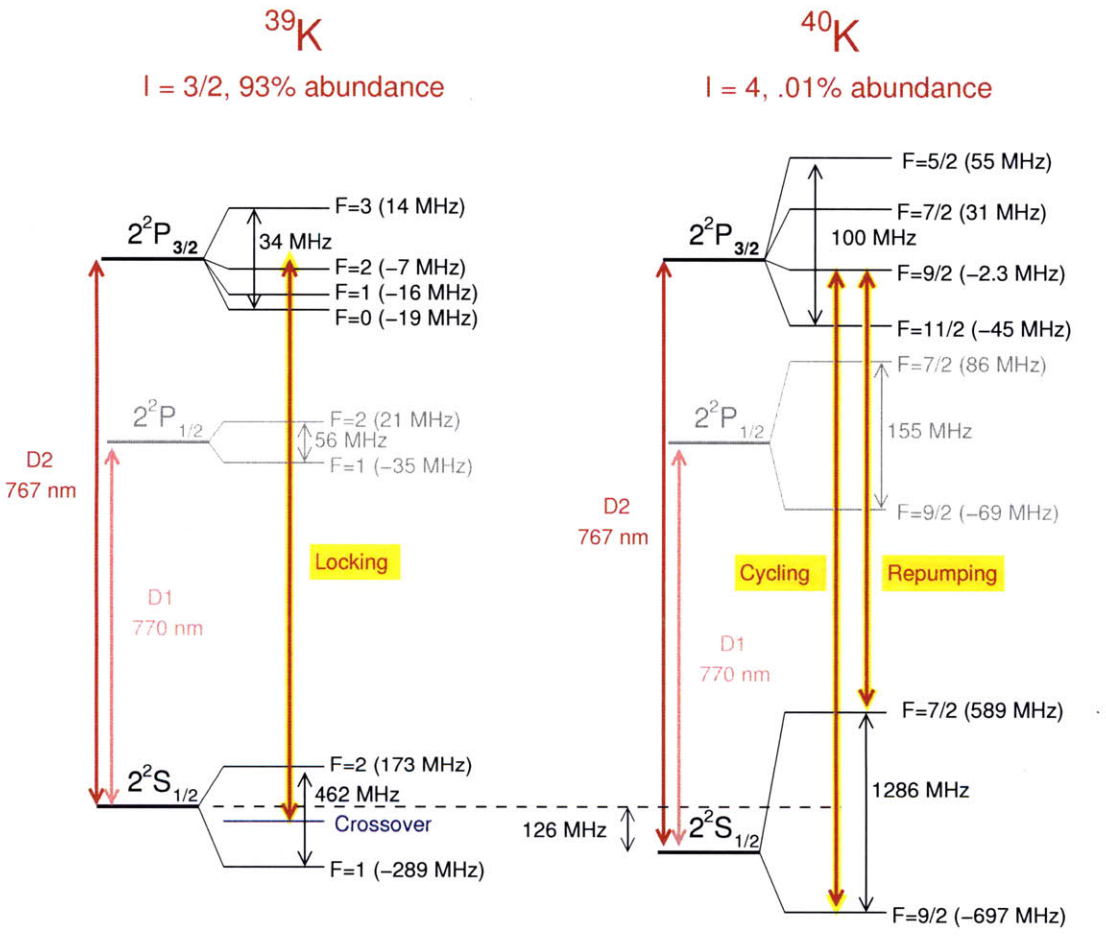

Figure 2-9: Hyperfine structure and relevant transitions for the ^{39}K that we lock to and the ^{40}K we want to cool and control.

Chapter 3

Lithium and Potassium Laser Systems

3.1 Grating-Stabilized Diode Lasers

We often want to our lasers to interact resonantly with atoms, so we want to stabilize the laser so that the variance in laser frequency is less than the linewidth Γ of an atomic transition. This means that we need to stabilize the frequency to within 1 MHz on top of 500 THz! We stabilize the laser frequency by giving the laser diode head active feedback from a variable-angle diffraction grating and also by modulating the current. The basic setup is shown in figures 3-1 and 3-2. A laser diode head sits inside a collimation package with a collimating lens that is adjusted to collimate the diverging beam. The collimation package sits inside some housing which sits on top of the cold side of a thermo-electric cooler (TEC). The other side of the TEC is connected to a large aluminum heat sink. A diffraction grating and a mirror sit parallel to each other on a mount that is attached to the moving side of a mirror mount.

We change θ, the angle between the incoming laser beam and the diffraction grating normal, by applying a voltage to a piezo-electric transducer (PZT) that pushes on the lever arm with the grating. As shown in figure 3-1, a mirror parallel to the diffraction grating on the same lever arm ensures that the angle of the outgoing beam does

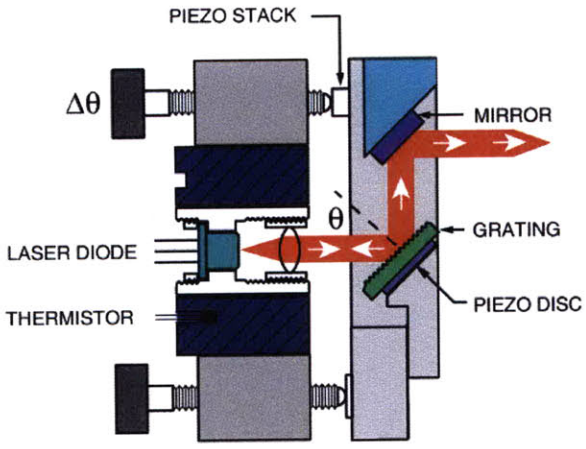

Figure 3-1: Schematic of laser. From [16].

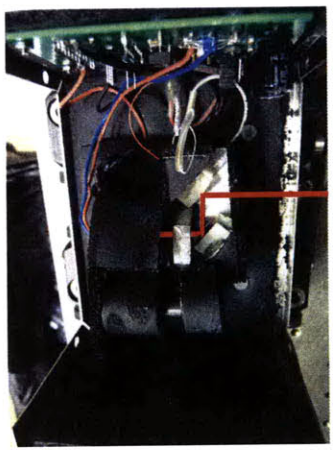

Figure 3-2: Real laser.

not vary with the PZT length[16]. We can also change the wavelength by changing the temperature and current of the diode laser. Changing the temperature changes the cavity length and also shifts the gain profile of the laser[14]. Changing the current also changes the temperature and also changes the charge carrier density, which changes the index of refraction of the semiconductor[14]. The laser frequency can change much more quickly with the current than it can with the TEC temperature.

The diffraction grating gives two kinds of feedback, which we will call cavity feedback and grating feedback. We align the diffraction grating in the Littrow configuration so that the -1st order diffraction order travels back into the laser diode head. Cavity feedback picks out light of wavelength λ such that the round-trip path length $2L = n\lambda$ interferes constructively when it returns to the laser cavity. The free spectral range $\Delta\nu_{\mathrm{FSR}} = c/2L$ is the spacing between allowed frequencies. In addition, we have grating feedback because in the Littrow configuration, the wavelength is such that $\lambda = 2d\sin\theta$, where d is the spacing between the grating lines, and θ is the angle between the incident light and the normal to the diffraction grating as shown in figure 3-1. For both the lithium and potassium lasers, we use a Thorlabs GR13-1208 ruled diffraction grating with 1800 lines/mm. Plugging in $\lambda_{\mathrm{Li}} = 671$ nm and $\lambda_{\mathrm{K}} = 767$ nm gives $\theta_{\mathrm{Li}} \approx 37.1$ degrees and $\theta_{\mathrm{K}} \approx 43.7$ degrees.

Here we show that $\Delta\lambda/\lambda$ is inversely proportional to the number of diffraction

grating lines N that are illuminated. Let d be the distance between the grating lines, θ be the angle between the grating normal and the line from the grating to the observation point. The phase difference between the light from adjacent lines is,

$$\delta = \frac{2\pi}{\lambda} d \sin\theta. \tag{3.1}$$

From summing a geometric series of phases $e^{in\delta}$ and recognizing $\sin x = \frac{1}{2}(e^{ix} - e^{-ix})$, we know that N sources give the interference pattern[7],

$$I = I_0 \left[\frac{\sin(N\delta/2)}{\sin(\delta/2)}\right]^2. \tag{3.2}$$

There is also a much broader single-slit diffraction envelope that the interference profile falls under, but since we just want the linewidth, we can just consider N source interference. The principal maxima occur when the denominator vanishes[7]. At the first diffraction order, $\delta/2 = \pi$, so $\sin\theta = \lambda/d$. The angles of the first diffraction order for two different wavelengths λ and $\lambda + \Delta\lambda$ are $\theta \approx \sin\theta = \lambda/d$ and $\theta + \Delta\theta \approx \sin(\theta + \Delta\theta) = (\lambda + \Delta\lambda)/d$. The angular separation between the two first diffraction orders is $\Delta\theta = \Delta\lambda/d$. By the Rayleigh criterion, the minimum separation between the interference patterns so that they can still be resolved is when the first minimum of one pattern overlaps with the maximum of the other. The first minimum occurs when $N\delta/2 = \pi$, so when $\theta \approx \sin\theta = \lambda/Nd$. Setting this equal to the angular separation gives $\Delta\lambda/d = \lambda/Nd$, and therefore,

$$\frac{\Delta\lambda}{\lambda} = \frac{1}{N}. \tag{3.3}$$

Assuming that the Rayleigh criterion is a good approximation to the angular spread of first diffraction orders that travel back to the diode laser head, equation (3.3) gives us the linewidth of the grating feedback.

Now we do some further analysis to compare the cavity and grating feedback. Let $\Delta\lambda$ and $\Delta\nu$ be the wavelength and frequency spreads under the amplitude vs. wavelength and frequency profiles given by the cavity and grating feedback. From

$\lambda = c/\nu$, we find that $\Delta\lambda = -c\Delta\nu/\nu^2$. So we find that,

$$\left|\frac{\Delta\lambda}{\lambda}\right| = \left|\frac{\Delta\nu}{\nu}\right|. \tag{3.4}$$

We know that $\Delta\lambda/\lambda = 1/N = \Delta\nu/\nu$. The width of the diffraction grating that will be illuminated is approximately $2w$ where w is the waist of the Gaussian laser beam. So for a 5 mm beam width and 700 nm light,

$$\Delta\nu_{\text{grating}} = \frac{\nu}{N} = \frac{c}{\lambda \cdot 1800\frac{\text{lines}}{\text{mm}} \cdot 5 \text{ mm}} \approx 50 \text{ GHz}. \tag{3.5}$$

In order to avoid mode-hopping, we want $\Delta\nu_{\text{FSR}}$ to be not more than an order of magnitude smaller than $\Delta\nu_{\text{grating}}$, where $\Delta\nu_{\text{FSR}} = c/2L$, so,

$$L < \frac{c}{2 \cdot 50 \text{ GHz}} \approx 3 \text{ cm}, \tag{3.6}$$

which is close to our current cavity length.

In addition, we want the cavity feedback and the grating feedback to move at the same rate when we sweep the frequency so that we stay on the same mode. Here we do the calculation for the simple case where the grating face lies along the pivot arm, as shown in figure 3-3. The more general case is messy and gives a similar desired pivot length. Let α be the angle between the pivot arm and the vertical, R be the length of the pivot arm, θ be the angle between the laser beam and the grating normal, and L be the length of the cavity between the grating and the diode. When we change α, we want the peak wavelength from both kinds of feedback to be the same,

$$\frac{d\lambda_{\text{grating}}}{d\alpha} = \frac{d\lambda_{\text{cavity}}}{d\alpha}. \tag{3.7}$$

Plugging in wavelengths of the light from the two kinds of feedback gives,

$$\frac{d}{d\alpha}\left(2d\sin\theta\right) = \frac{d}{d\alpha}\left(\frac{2L}{n}\right), \tag{3.8}$$

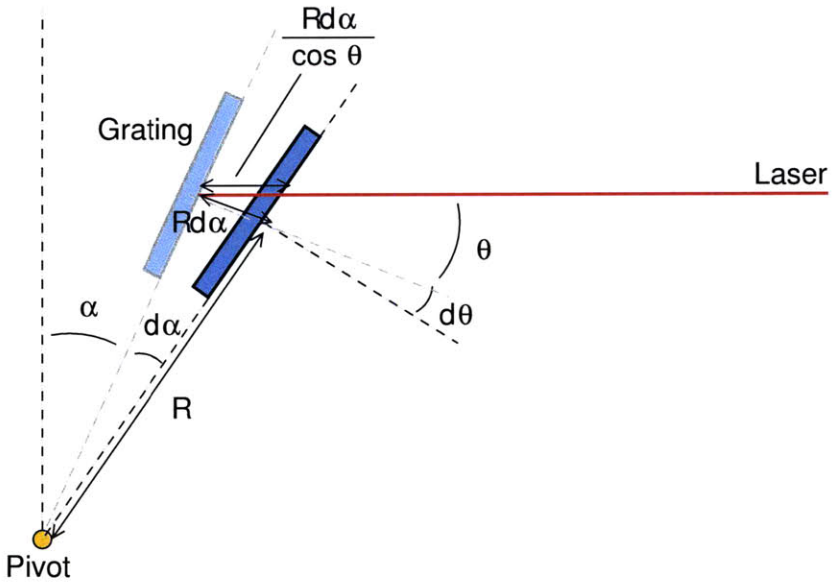

Figure 3-3: Geometry of the laser beam, diffraction grating and pivot point.

so,

$$\frac{dL}{d\alpha} = nd\cos\theta\frac{d\theta}{d\alpha} \tag{3.9}$$

As shown in figure 3-3 we find that $dL = Rd\alpha/\cos\theta$, so

$$\frac{dL}{d\alpha} = \frac{R}{\cos\theta}. \tag{3.10}$$

If we sum the angles along the horizontal laser line, we find $(90-\alpha)+90+\theta = 180$, so $\theta = \alpha$. Plugging the derivatives into the condition (3.9) gives,

$$\frac{R}{\cos\theta} = nd\cos\theta = \frac{2Ld}{\lambda}\cos\theta \tag{3.11}$$

We then substitute $n = 2L/\lambda$ and $\cos\theta = \lambda/2d$ and solve for R,

$$R = \frac{2Ld}{\lambda}\cos^2\theta = \frac{2Ld}{\lambda}\frac{\lambda^2}{4d^2} = \frac{L\lambda}{2d} \approx \frac{700\text{ nm}}{2\cdot 1\text{ mm}/1800\text{ lines}} \approx 1.3L. \tag{3.12}$$

3.2 Saturated Absorption Spectroscopy

We want to lock our laser to the frequency of a single atomic transition. The atoms in our vapor cell move with a random velocity distribution, so as we sweep the laser frequency to do spectroscopy, the laser comes into resonance with different velocity groups of atoms. In the absorption spectrum, each sharp Lorentzian resonance for a stationary atom becomes Doppler-broadened into a Gaussian approximately 600 MHz wide for our potassium vapor cell, which is large enough to obscure any hyperfine structure. To overcome Doppler broadening, we use counterpropagating pump and probe beams to select out particular velocity classes of atoms. Here we describe how saturated absorption spectroscopy works for a system like Li or K with two ground states $|g_1\rangle$ with degeneracy 4 and $|g_2\rangle$ with degeneracy 2 and one excited state $|e\rangle$, shown in figure 3-4. In this system, we start with twice as many atoms in the $|g_1\rangle$ state as in the $|g_2\rangle$ state. Let the transition frequencies be ω_1 and ω_2. This is the case for the lithium and potassium D2 lines that we will lock to, as the hyperfine levels of the excited state are so close together that they are essentially degenerate.

Let the laser have frequency ω in the lab frame. If an atom is moving with velocity v, it sees the pump beam at frequency $\omega + kv$ and the probe beam at frequency $\omega - kv$. We can only see features when the pump changes the atom number of the velocity class that the probe is on resonance with, which happens when both the pump and the probe are on resonance with the same velocity group of atoms. There are two transitions, so either the pump and probe are on resonance with the same transition and we look at the $v = 0$ class of atoms, or the pump and the probe are on resonance with different transitions and we look at the $v = \pm(\omega_2 - \omega_1)/k$[35].

When the lasers probe the zero velocity class at frequency ω_1, atoms are continually excited out of the $|g_1\rangle$ state and into the $|e\rangle$ state where they then decay to one of the two ground states. When they decay to $|g_2\rangle$ they stay there. So we are simply optically pumping the atoms to the $|g_2\rangle$ state and depleting the population in the $|g_1\rangle$ state. Therefore, when the probe beam sees fewer atoms at $|g_1\rangle$ than normal, so we see a peak in the probe signal because less light will be absorbed. The same is the

case for when the lasers probe the zero velocity class at frequency ω_2.

When the lasers probe the $\pm(\omega_2 - \omega_1)/k$ velocity classes at frequency $(\omega_2 - \omega_1)/2$, the atoms see the pump at frequency ω_1 and the probe at frequency ω_2, or vice-versa for the other sign of the velocity. In both cases, the pump beam pumps the atoms over to the ground state that the probe is probing, and the probe will see more atoms at that ground state than normal. Therefore, we will see a dip in the probe signal because more light will be absorbed.

3.3 Frequency-Modulation Spectroscopy

We want to lock the laser frequency on the peak of the crossover resonance. However, the Lorentzian-shaped peak is symmetric, so we cannot tell from the absorption signal value whether the frequency is too high or too low. The solution is to use frequency-modulation (FM) spectroscopy, where we modulate the frequency of the probe beam, perform some signal processing, and get an anti-symmetric error signal that we will be able to lock to.

3.3.1 Electro-Optical Modulators

Theory of Operation

To modulate the laser frequency, we pass the laser beam through an electro-optical modulator (EOM), shown in figure 3-5. The EOM consists of an simple inductor made from about 10 loops of wire and a capacitor made from two pieces of copper solder wick on either side of a crystal. These are wired in a series LC circuit and RF power from the EOM driver is coupled in through a BNC cable. The voltage across the capacitor oscillates and produces an oscillating electric field inside the crystal. The oscillating electric field makes the index of refraction of the light oscillate in time, $n = n_0 + n_1 \sin \omega_m t$. When the light is polarized along the crystal's extraordinary axis, we have the best phase modulation. (However we have still gotten 100 mV peak to peak error signals with crystals with the wrong polarization! After this exercise

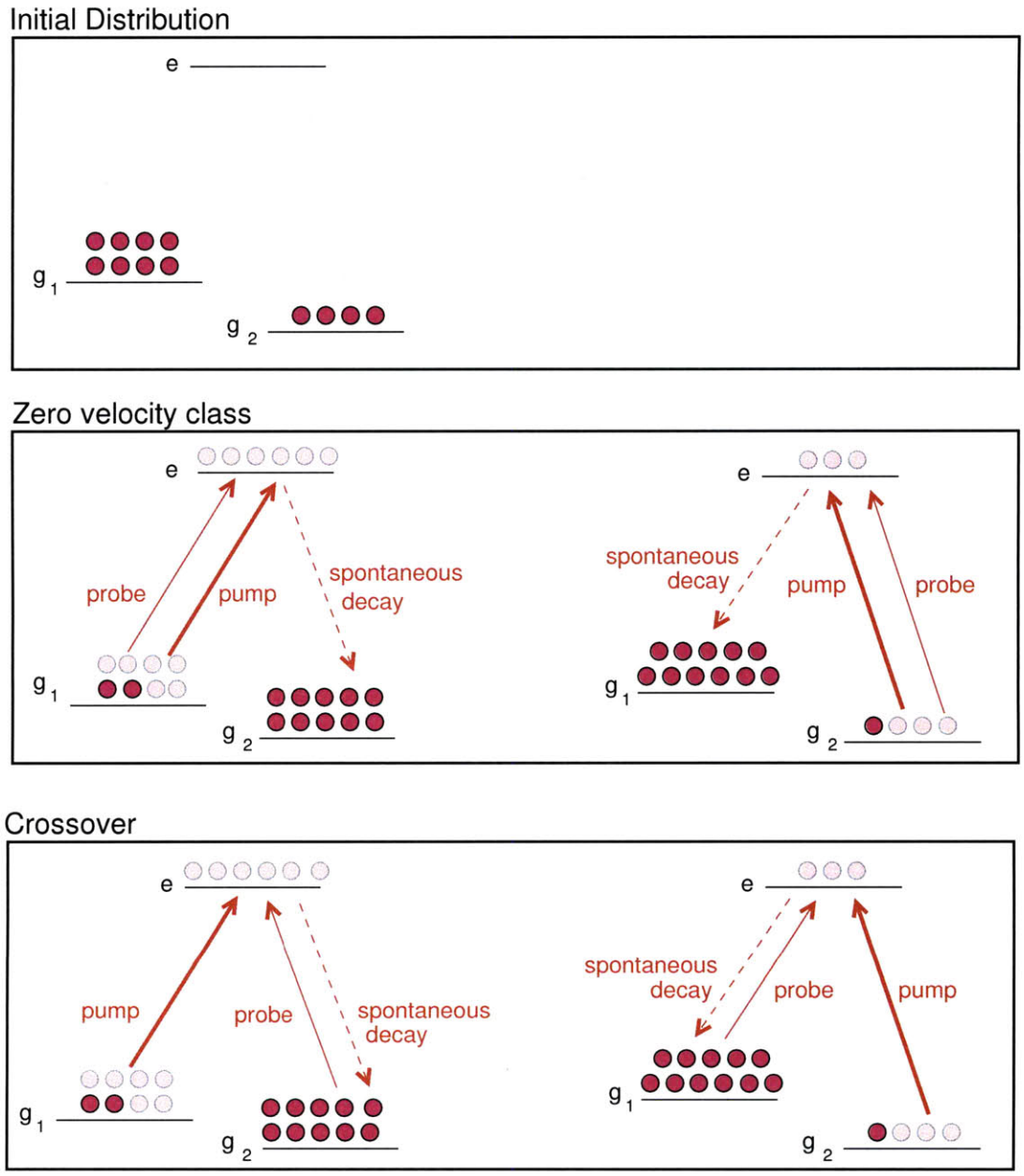

Figure 3-4: Illustration of saturated absorption spectroscopy in a system with two ground states and one excited state.

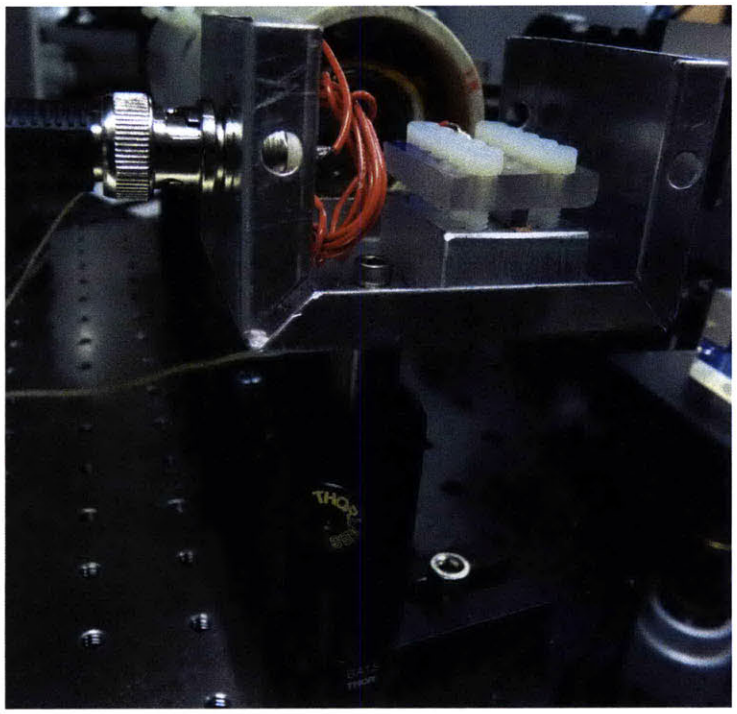

Figure 3-5: Electro-optical modulator. The pink wire forms the inductor and the crystal is under the plexiglass between the two sets of screws.

it is shockingly easy to get the error signal with the correct crystal!) Therefore, the phase that the laser acquires by oscillating in time,

$$2\pi nL/\lambda = 2\pi(n_0 + n_1 \sin \omega_m t)L/\lambda \tag{3.13}$$

also oscillates in time.

Construction

In order to make really good electrical contact with the electrodes of the crystal, we used copper braids from solder wick (Marko Cetina's awesome idea) - they are just the right width and then are more flexible so they fill in the space better and are less likely to break the crystal. First we put a chunk of metal down for a heat sink, then a copper braid, then the crystal, then another copper braid. The bottom copper braid is not necessary because the metal heat sink is already there, but it might help make

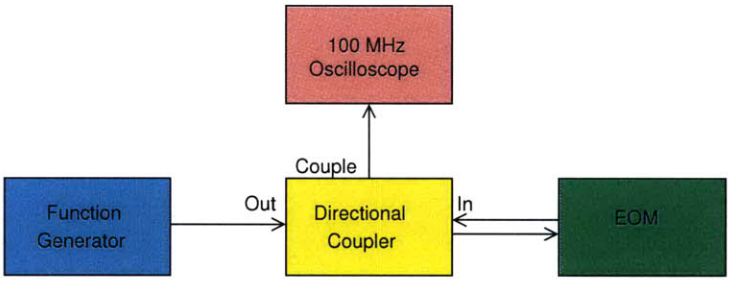

Figure 3-6: Block diagram of the setup to tune the resonance of the EOM.

better electrical contact if there are dents or scratches in the heat sink. Everything is held in place with a piece of plexiglass on top, secured to the heat sink with many small, closely spaced 6-32 screws. Plastic screws were used to limit the force on the crystal so it would not break, plus they would act like ten little antennas and change things. In order to regularly space the screws for equal pressure application, a mill with digital readout was used to do the drilling. A BNC connector that grounds right to the box was used for a good ground connection. Then the middle pin was soldered to a coil of wire soldered to the top copper braid. The bottom copper braid was grounded via the box.

Tuning the LC Circuit

Our goal was to transfer energy efficiently by making a resonant LC circuit, where L is a hand-wound coil and the C is the electrodes of the crystal and the copper braids. We used a directional coupler to look at the reflected RF and minimize it by changing the number of windings in the capacitor and also the frequency. The setup to observe the resonances is shown in figure 3-6. The reflection amplitude is minimized at the resonant frequencies. You can have the function generator sweep the frequency and look at the reflection amplitude vs. frequency profile on the oscilloscope to find minima. We first unplugged the EOM to look at the background profile, which had bumps in this profile because of the different frequency responses of the components. When we plugged in the EOM, additional dips appeared, which were the true resonances.

3.3.2 RF Signal Manipulation

The following derivation follows Bjorklund's in [10] and fills in some more steps. When we pass a laser beam with electric field $E_0 e^{i\omega_0 t}$ through an EOM, the output signal is phase-modulated so it becomes[33],

$$E = E_0 e^{i(\omega_c t + M\sin(\omega_m t))}. \tag{3.14}$$

Because M is small, we can Taylor expand, $e^{iM\sin\omega_m t} \approx 1 + iM\sin\omega_m t$, so

$$E = E_0 e^{i\omega_c t}(1 + M\sin\omega_m t). \tag{3.15}$$

We can write $\sin\omega_m t$ as $(e^{i\omega_m t} - e^{-i\omega_m t})$ and so we have,

$$E = E_0(e^{i\omega_c t} + \frac{M}{2}e^{i(\omega_c+\omega_m)t} + \frac{M}{2}e^{i(\omega_c-\omega_m)t}). \tag{3.16}$$

So we see that modulating the laser phase at frequency ω_m adds sidebands at $\omega_c - \omega_m$ and $\omega_c + \omega_m$. We write the frequencies as $\omega = \omega_c + n\omega_m$ where $n = -1, 0, 1$.

Then we pass the signal through a vapor cell. At each step in length, the average number of photons that will be absorbed by the vapor is proportional to the total number of photons. Therefore, the intensity of the electromagnetic wave decays exponentially as a function of length. The decay constant is called the absorption coefficient and we label it α[10]. Also let the cell have length L and index of refraction η. α and η are functions of the laser frequency. Let $2\delta_n = \alpha L$ be the total intensity attenuation and $\delta_n = \alpha L/2$ be the total amplitude attenuation. Let $\phi_n = \eta_n L(\omega_c + n\omega_m)/c$ be the optical phase shift. Then we can multiply the frequency components of the initial field E by[10],

$$T_n = e^{-\delta_n - i\phi_n}, \tag{3.17}$$

to get the new electric field. So the transmitted field is,

$$E = E_0\left[T_0 e^{i\omega_c t} + T_1\frac{M}{2}e^{i(\omega_c+\omega_m)t} - T_{-1}\frac{M}{2}e^{i(\omega_c-\omega_m)t}\right]. \tag{3.18}$$

On a photodiode we observe the intensity $I \propto |E|^2 = E^*E$. M is small so we can eliminate all M^2 terms,

$$|E^2| \approx E_0^2 \left[T_0^* T_0 + T_0^* T_1 \frac{M}{2} e^{\omega_m t} - T_0^* T_{-1} \frac{M}{2} e^{-\omega_m t} + T_1^* T_0 \frac{M}{2} e^{-i\omega_m t} - T_{-1}^* T_0 \frac{M}{2} e^{i\omega_m t} \right]. \tag{3.19}$$

Plugging in for δ_n and ϕ_n and rearranging a bit gives,

$$\begin{aligned} E_0^2 \Bigg[& e^{(-2\delta_0)} + e^{(-\delta_0-\delta_1)+i(\phi_0-\phi_1)} \frac{M}{2} e^{i\omega_m t} - e^{(-\delta_0-\delta_{-1})+i(\phi_0-\phi_{-1})} \frac{M}{2} e^{-\omega_m t} \\ & + e^{(-\delta_1-\delta_0)-i(\phi_0-\phi_1)} \frac{M}{2} e^{-i\omega_m t} - e^{(-\delta_{-1}-\delta_0)-i(\phi_0-\phi_{-1})} \frac{M}{2} e^{i\omega_m t} \Bigg]. \end{aligned} \tag{3.20}$$

We can factor out some $e^{(-\delta_0-\delta_1)}$ and $e^{(-\delta_0-\delta_{-1})}$ terms and get,

$$\begin{aligned} E_0^2 \Bigg[& e^{-2\delta_0} + e^{-\delta_0-\delta_1} M \frac{e^{i((\phi_0-\phi_1)+\omega_m t)} + e^{-i((\phi_0-\phi_1)+\omega_m t)}}{2} \\ & - e^{-\delta_0-\delta_{-1}} M \frac{e^{i(-(\phi_0-\phi_{-1})+\omega_m t)} + e^{-i(-(\phi_0-\phi_{-1})+\omega_m t)}}{2} \Bigg], \end{aligned} \tag{3.21}$$

which factoring out $e^{-2\delta_0}$ and substituting in trigonometric formulas, we can write as,

$$E_0^2 e^{-2\delta_0} \left[1 + e^{\delta_0-\delta_1} M \cos((\phi_0 - \phi_1) + \omega_m t) - e^{\delta_0-\delta_{-1}} M \cos(-(\phi_0 - \phi_{-1}) + \omega_m t) \right]. \tag{3.22}$$

Using the angle addition formula and regrouping we at last have the formula in Bjorklund [10],

$$\begin{aligned} E_0^2 e^{-2\delta_0} \Big[1 + & \left[e^{\delta_0-\delta_1} \cos(\phi_1 - \phi_0) - e^{\delta_0-\delta_{-1}} \cos(\phi_0 - \phi_{-1}) \right] M \cos \omega_m t \\ & + \left[e^{\delta_0-\delta_1} \sin(\phi_1 - \phi_0) - e^{\delta_0-\delta_{-1}} \sin(\phi_0 - \phi_{-1}) \right] M \sin \omega_m t. \Big] \end{aligned} \tag{3.23}$$

If $|\delta_0 - \delta_1|, |\delta_0 - \delta_{-1}|, |\delta_0 - \delta_1|, |\delta_0 - \delta_{-1}| \ll 1$, then using the small angle approximation we get,

$$I(t) = \frac{cE_0^2}{8\pi} e^{-2\delta_0} [1 + (\delta_{-1} - \delta_1) M \cos \omega_m t + (\phi_1 + \phi_{-1} - 2\delta_0) M \sin \omega_m t]. \tag{3.24}$$

The FM spectroscopy condition as stated in [10] is that w_m is large compared to the

linewidth of the spectral feature so that when we sweep the laser frequency ω_c only one sideband, say the upper sideband, probes the feature. Therefore, α and η for the carrier and the lower sideband are constant.[10] In this case, δ_{-1} and δ_0 remain constant at the background absorption loss. $\bar{\delta}$ and ϕ_{-1} and ϕ_0 remain constant at the background phase shift $\bar{\phi}$. We note that the atoms do not give a background absorption loss or phase shift (and such a concept is totally wrong and nonsense), so these background numbers refer to the effects from the air, the glass in the cell, etc. Let $\Delta\delta = \delta_1 - \bar{\delta}$ and $\Delta\phi = \phi_1 - \bar{\phi}$. Then,

$$I(t) = \frac{cE_0^2}{8\pi}[1 - \Delta\delta M \cos\omega_m t + \Delta\phi M \sin\omega_m t]. \tag{3.25}$$

If we mix the photodiode signal $I(t)$ with a signal oscillating at the modulation frequency $A\cos(\omega_m + b)$, we get a signal proportional to

$$\Delta\delta \cos b + \delta\phi \sin b. \tag{3.26}$$

So we can choose to look at either the absorption δ as a function of the laser frequency ω_c or we can look at the dispersion ϕ as a function of the frequency, depending on the phase between the photodiode signal and the signal we beat it with.

3.3.3 EOM Driver

The block diagram for the EOM driver is shown in figure 3-7. The EOM drive signal begins at the voltage-controlled oscillator (VCO). The potassium EOM has a resonance frequency of $\approx$ 38 MHz and the lithium EOM has a resonance frequency of $\approx$ 29 MHz. The signal then passes through a splitter and half of it goes to the voltage-controlled attenuator. The control voltage comes from a resistor divider made with a potentiometer so that by turning a knob, you can tune the power. (In this situation we usually want as much RF power as possible, but with great power comes great noise so sometimes we want to turn it down slightly.) The signal then passes into the high-power amplifier and then it goes to drive the EOM.

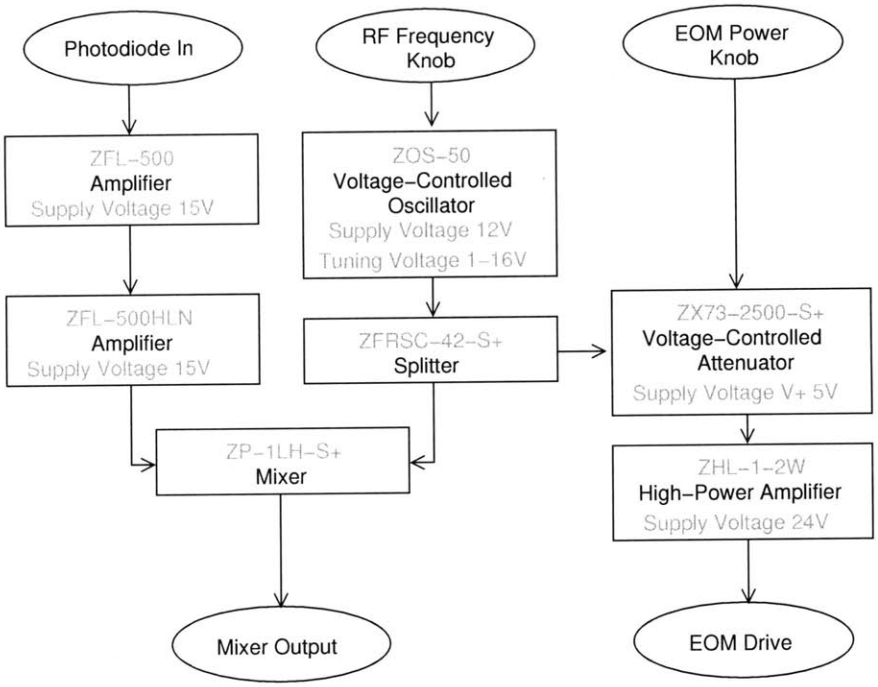

Figure 3-7: Electro-optical modulator driver block diagram, with Minicircuits part numbers and voltage specifications.

The other part of the VCO signal is mixed with the amplified saturated absorption spectroscopy signal from the photodiode. From equation (3.26) in the previous section, we know that we can vary the quadrature (absorption or dispersion) of the photodiode signal by varying the phase of the VCO signal. We can vary the relative phase by changing cable lengths or by changing the frequency, which will change how many oscillations happen within a fixed cable length.

3.4 Locking the laser

Given the antisymmetric error signal given by the dispersive quadrature of the FM spectroscopy signal, we want to apply proportional and integral feedback to the laser so that it will work to stay at the zero error point. To do this, we use the lockbox shown in figures 3-13 and 3-14. The proportional gain goes to the current modulation input on the current controller. The integral gain goes to the PZT on the laser. You

Figure 3-8: Front of the EOM driver box.

Figure 3-9: Voltage regulators and heat sinks.

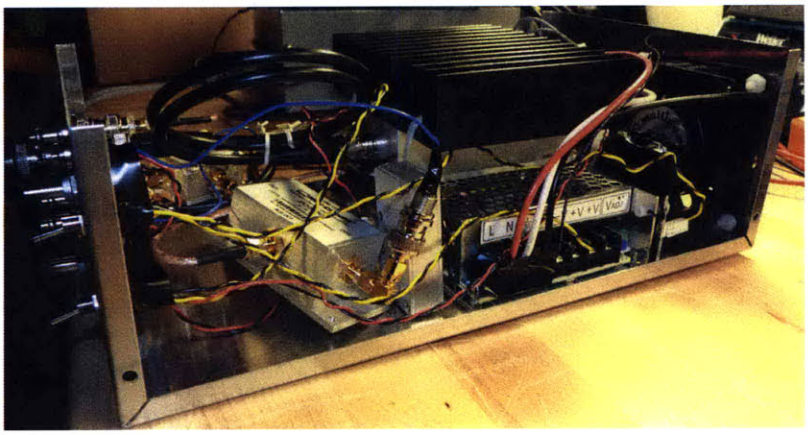

Figure 3-10: Inside the EOM driver box. There is a 24V power supply and voltage regulators to supply 5, 12 and 15 volts.

watch the error on the error monitor output and tune the offset knob so that the zero of the error signal is exactly at the peak of the crossover resonance.

The latest (as of 5/18/2010) version of the circuit and corresponding PCB that control the lockbox are shown in figures 3-11 and 3-12.

The error signal from the EOM driver "mixer out" port is fed into the "error signal in," and then passes through the LF347N which is a buffer. We can modulate the error signal in through "ERROR MOD" which passes through the INA114P which is a high-impedance buffer used for isolation. The ERROR MOD port is useful for testing the feedback loop because it lets us put in whatever frequency noise we want to we can test for terrible resonances in our circuit. We can also set the error signal offset with the ERR OFFSET potentiometer. The original error signal, the offset, and the modulation signal are summed at the second LF347N op-amp which is set up as an adder. The result of the sum is the error signal that we lock to. The error signal is passed through another LF347N buffer and then goes out where we can monitor it on a scope. The error signal is also passed to the proportional and integral feedback parts of the circuit.

When the lockbox is in scan mode, SWITCH1, SWITCH2 and SWITCH3 are closed. When SWITCH1 is closed, the output of the integral gain op-amp IC3A is ground. Then an external sawtooth wave is passed through a voltage divider made with a potentiometer for variable amplitude and then to the RAMP input. When SWITCH2 is closed, this signal reaches IC3B, which acts as an adder, adding the ramp signal, an offset signal from OUT OFFSET and the ground signal from IC3A. This is then the INT OUTPUT signal which goes to the PZT to scan the laser frequency.

When the lockbox is in lock mode, SWITCH1, SWITCH2 and SWITCH3 are open. In this case, IC3C is set up as an inverting amplifier with gain $R_{\mathrm{P,pot}}/R14$, where $R_{\mathrm{P,pot}}$ is set by the potentiometer attached to the PROP GAIN connector. The signal then passes through IC3D which implements a sign change on the proportional output by flipping SIGN CHANGE. IC3A is set up as an inverting integrator with[18],

$$V_{\mathrm{out}} = -\int_0^t \frac{V_{\mathrm{in}}}{(R_{\mathrm{I,pot}} + R4)C} dt + V_{\mathrm{initial}}. \tag{3.27}$$

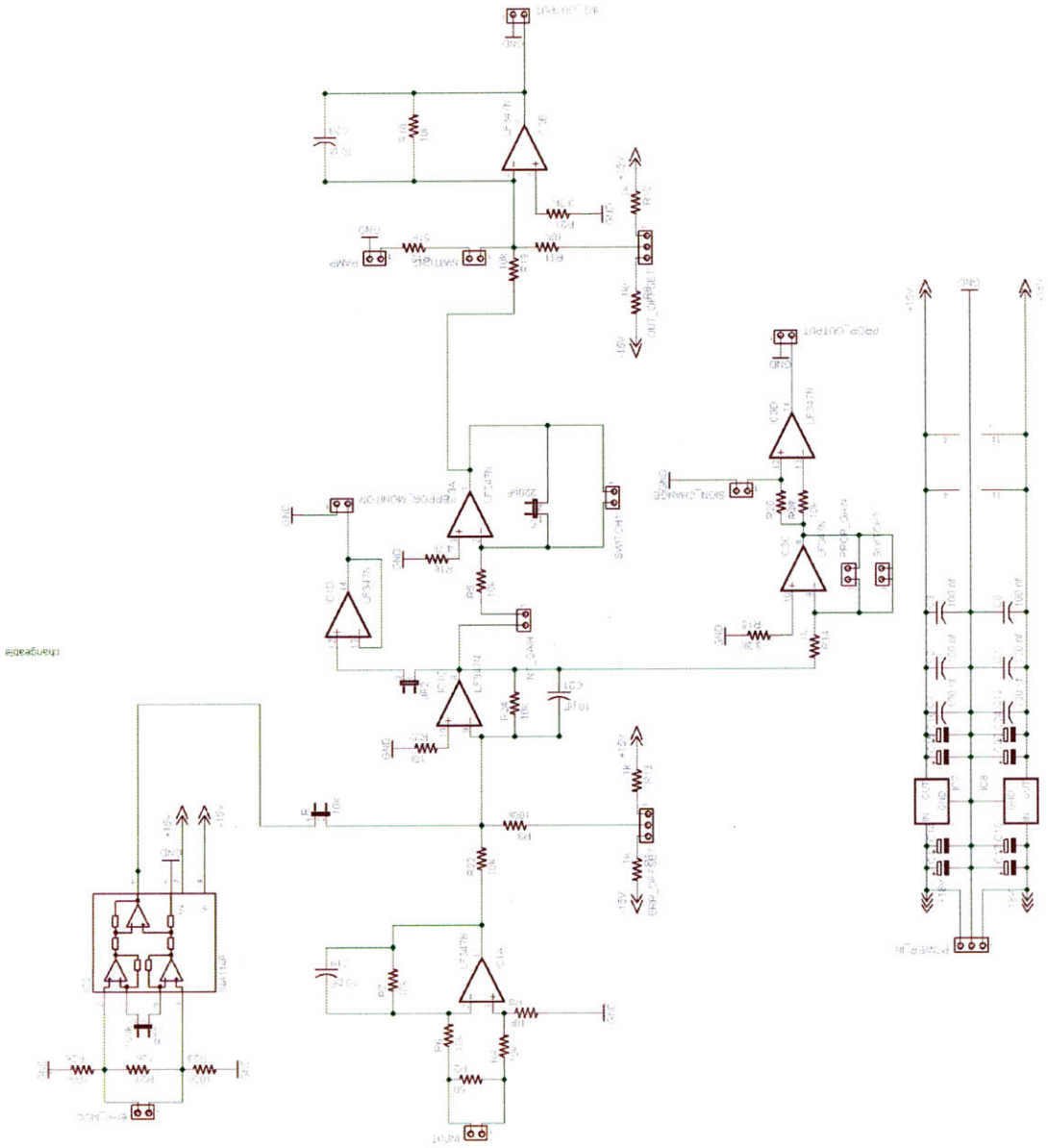

Figure 3-11: Updated schematic of the PI lockbox for diode laser frequency stabilization.

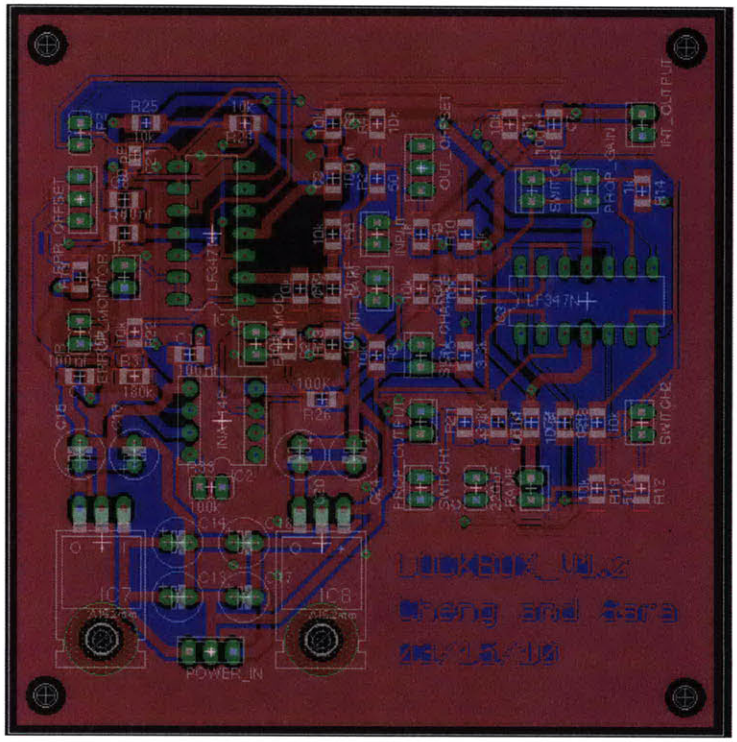

Figure 3-12: Updated PCB of the PI lockbox for diode laser frequency stabilization.

Figure 3-13: Front of the lockbox.

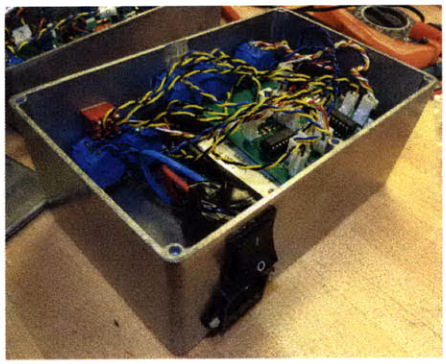

Figure 3-14: Inside the lockbox. We include a small power ±15V power supply inside the box.

where $R_{\mathrm{I,pot}}$ is set by the potentiometer attached to the INT GAIN connector. Note that $R_{\mathrm{P,pot}}$ is in the numerator, while $R_{\mathrm{I,pot}}$ is in the denominator, so to make both potentiometers increase the gain when you turn them clockwise, you need to hook them up in opposite ways.

3.5 Shifting the Frequency

3.5.1 Double Pass AOMs

We usually lock our lasers to the D2 crossover resonance for the most abundant isotope in our cell, which is ^{39}K in the Thorlabs potassium cell and ^{6}Li in our homebuilt cell made with enriched lithium. We use acousto-optical modulators (AOMs) in the double pass configuration to obtain all of the laser frequencies we want. The AOMs are composed of a crystal attached to a transducer. We couple in RF power to that makes the transducer oscillate, exciting sound waves (phonons) inside the crystal. We can describe how the AOM modifies light by photon-phonon scattering.[12][35] Let ω and Ω be the angular frequencies of the phonon and photon, respectively. Let $\vec{k}$ and $\vec{K}$ be the wavenumbers of the phonon and photon, respectively. As in [12], let the subscripts $i1$ and $d1$ denote the first incident and deflected beams and let $i2$ and $d2$

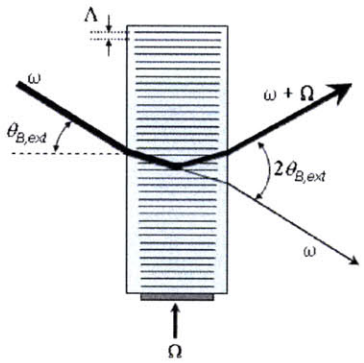

Figure 3-15: Diagram of an incident laser beam being frequency-shifted and deflected by an acousto-optical modulator. Image from [12].

denote the second incident and deflected beams. Then,

$$\omega_{d1} = \omega_{i1} \pm \Omega \tag{3.28}$$

$$\vec{k}_{d2} = \vec{k}_{i1} \pm \vec{K}. \tag{3.29}$$

If we reflect the deflected beam and put it back through the AOM along the undeflected beam path, $\omega_{i2} = \omega_{i1}$ and $\vec{k}_{i2} = -\vec{k}_{d1}$. The photons that absorb a phonon are again deflected and we find,

$$\omega_{d2} = \omega_{i2} \pm \Omega = (\omega_{i1} \pm \Omega) \pm \Omega = \omega_{i1} \pm 2\Omega \tag{3.30}$$

$$\omega_{d2} = \vec{k}_{i2} + \vec{K} = (-\vec{k}_{i1} \mp \vec{K}) \pm \vec{K} = -\vec{k}_{i1}. \tag{3.31}$$

So the angle of deflection is independent of the RF frequency Ω.

3.5.2 AOM Driver

The block diagram for the AOM driver is shown in figure 3-16. On/off, frequency and power of the drive signal are set up so that they can be controlled internally or externally. The external controls are BNC cables on the outside of the box and the internal controls are an on/off switch and voltage dividers with potentiometers for the power and frequency. The drive signal begins at the VCO, then it goes to

a voltage-controlled attenuator, then it goes to a switch where we control whether or not it comes out. The potassium AOM drivers I built use ZMSW-1211 switches, which are good because they are cheap, but bad because they allow some RF to leak through and also require conjugate control signals, hence the inverter. In the future, I recommend using ZASWA-2-50DR+ which is TTL driven and has better isolation. After the switch, the signal goes into the 2 watt amplifier and then to the AOM.

Some advice I have is to put 4 or more AOM drivers in a single box, as shown in figures 3-17 and 3-18. Put a 24 V power supply that can power your amps (they need at least 1 amp each) inside the box so that the box can plug directly into the wall. For the other 5, 12 and 15 volt supplies that are required, particularly the ones that supply a control voltage to the VCOs, we should use a large external power supply for the entire lab. That way, if the voltages vary over time, they will vary identically for all the boxes in the lab. Put the amplifier heat sinks in the box so they don't radiate around the whole room. Also, test your power supply outputs before hooking them up to components. The PowerOne power supplies have a circular metal component that pokes through the back and you should electrical tape over them so they do not short to ground via the metal box. Put at least one or two fans in the box. Make sure air blows over your amp heat sinks, power supplies and voltage regulator heat sinks.

3.6 Lithium System and Data

The schematic of the lithium laser system is shown in figure 3-19. The master laser is placed far away from the hot vapor cell. Light from the master laser passes through a 60 dB optical isolator. The light is initially vertically polarized. We use a 1/2 waveplate and a polarizing beam splitter, which lets horiziontally polarized light through and reflects vertically polarized light, to control how much light goes to spectroscopy for locking and how much goes to seed the tapered amplifiers (TAs). When doing saturated absorption spectroscopy, rather than using a beamsplitter to make the pump and probe beams, we retroreflect the pump beam to get the probe

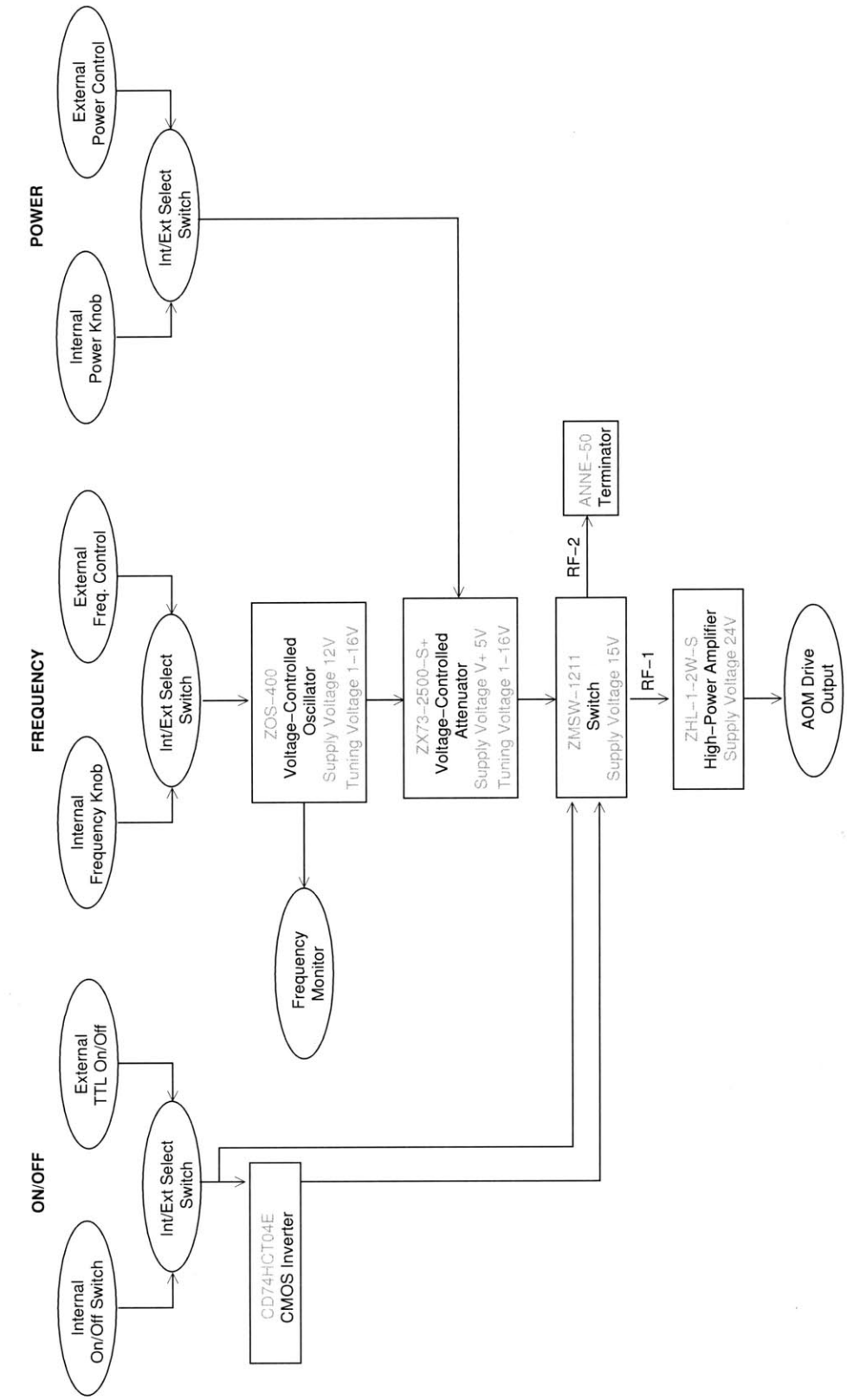

Figure 3-16: Potassium AOM driver schematic.

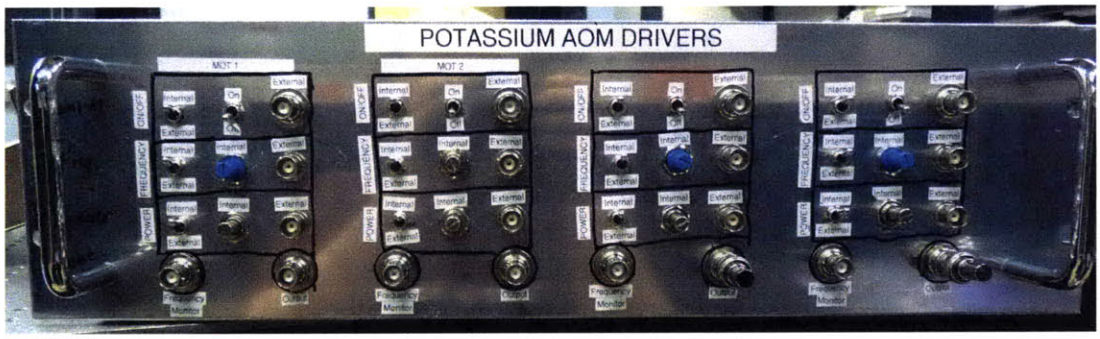

Figure 3-17: Front of the potassium AOM driver box, capable of driving 4 AOMs.

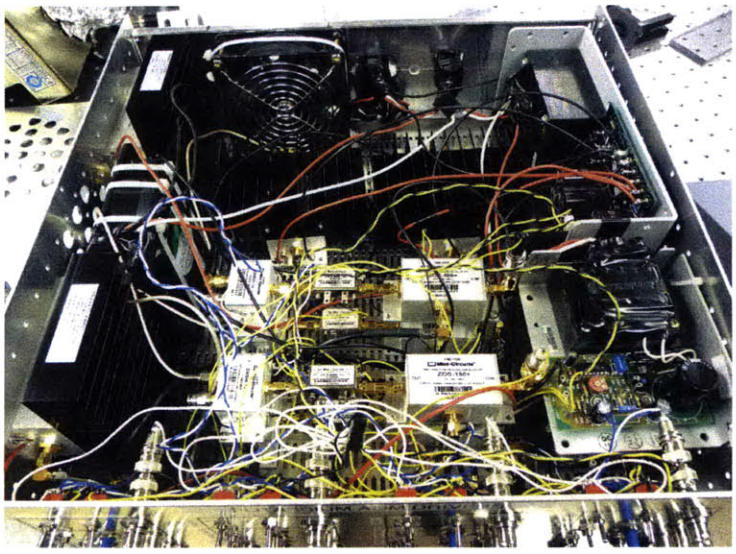

Figure 3-18: Inside of the potassium AOM driver box.

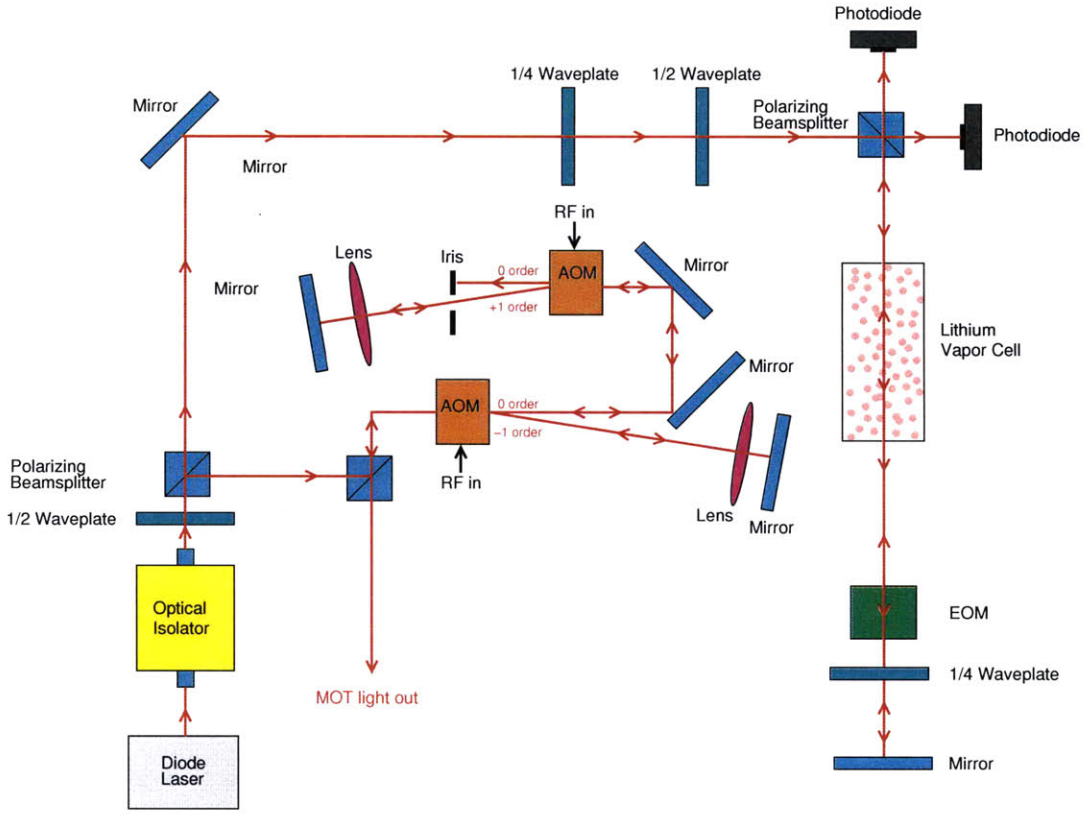

Figure 3-19: Lithium laser system.

beam so that we need to use less power for locking. For FM spectroscopy, we modulate the probe beam and observe the probe beam using a photodiode fast enough to see the $\approx$ 30 MHz modulations. The lithium vapor cell is shown in figure 3-20. We control how much lithium is in vapor form by controlling the temperature of the cell using a variac and a heating band wrapped around the middle of the cell where the solid lithium is. We want enough vapor so that we have a strong absorption signal, but not so much that the probe beam is completely absorbed at some frequencies and the tip of the Doppler-broadened spectrum gets clipped off and the spectra start to saturate. We found that the best temperature for this particular cell is around 340^{o}C. The length of the lithium cell is chosen so few lithium vapor atoms reach the viewports, so the viewports are coated very slowly in time. Also to prevent coating of the viewports, we put argon buffer gas in the cell to reduce the mean free path of the lithium atoms. The lithium D2 line and corresponding error signal are shown in

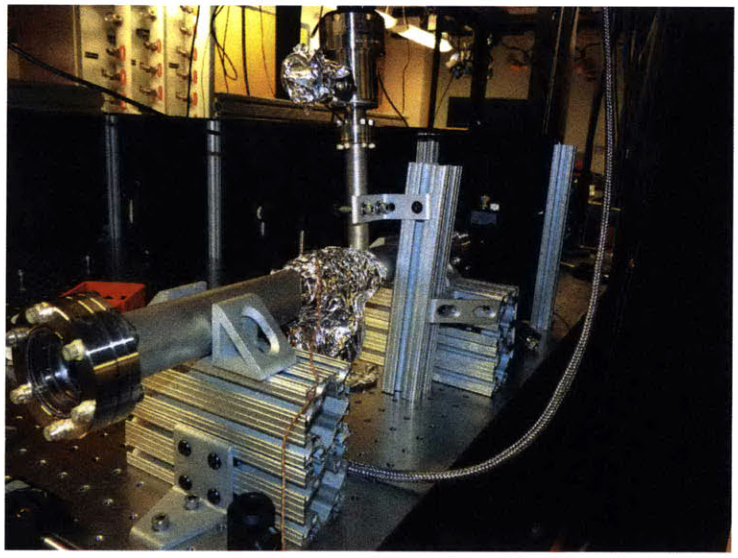

Figure 3-20: Lithium cell.

figure 3-21.

3.7 Potassium System and Data

The potassium laser system is shown in figure 3-22. As in the lithium laser system, the master laser is placed far away from the warm vapor cell. Most of the light goes to seed the TAs and the rest is used for spectroscopy to lock the laser. The photodiode chip and the EOM aperture are both much smaller than the original beam size, so we used two lenses in a telescope configuration to reduce the beam size for spectroscopy. We do not also reduce the seed light beam size because if we want to seed a slave laser by injection locking, it is important that the input and output beams are similar in size for better mode-matching. We did not use the trick of retroreflecting the beam for saturated-absorption spectroscopy, but that would be a good power-saving potential upgrade. The potassium cell is shown in figures 3-23 and 3-24. We used a Thorlabs glass cell and made a homemade heating enclosure for it. The atoms will stick on the coldest part of the cell, so it is key that our enclosure keeps the ends of the cell as hot as the length of the cell. Our solution was to heat the cell rather indirectly.

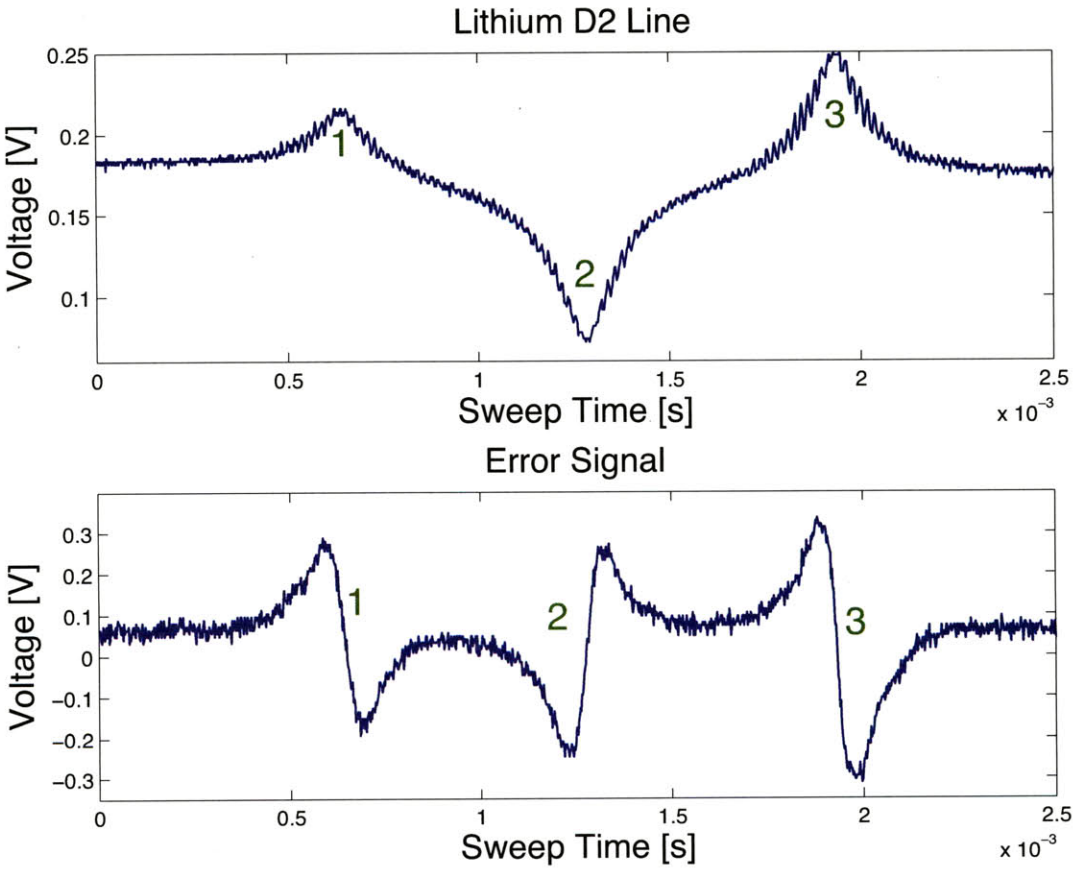

Figure 3-21: Lithium D2 line and error signal. 1 is the $2^2S_{1/2}, F = 1/2 \rightarrow 2^2P_{3/2}$ transition, 2 is the crossover resonance and 3 is the $2^2S_{1/2}, F = 3/2 \rightarrow 2^2P_{3/2}$ transition.

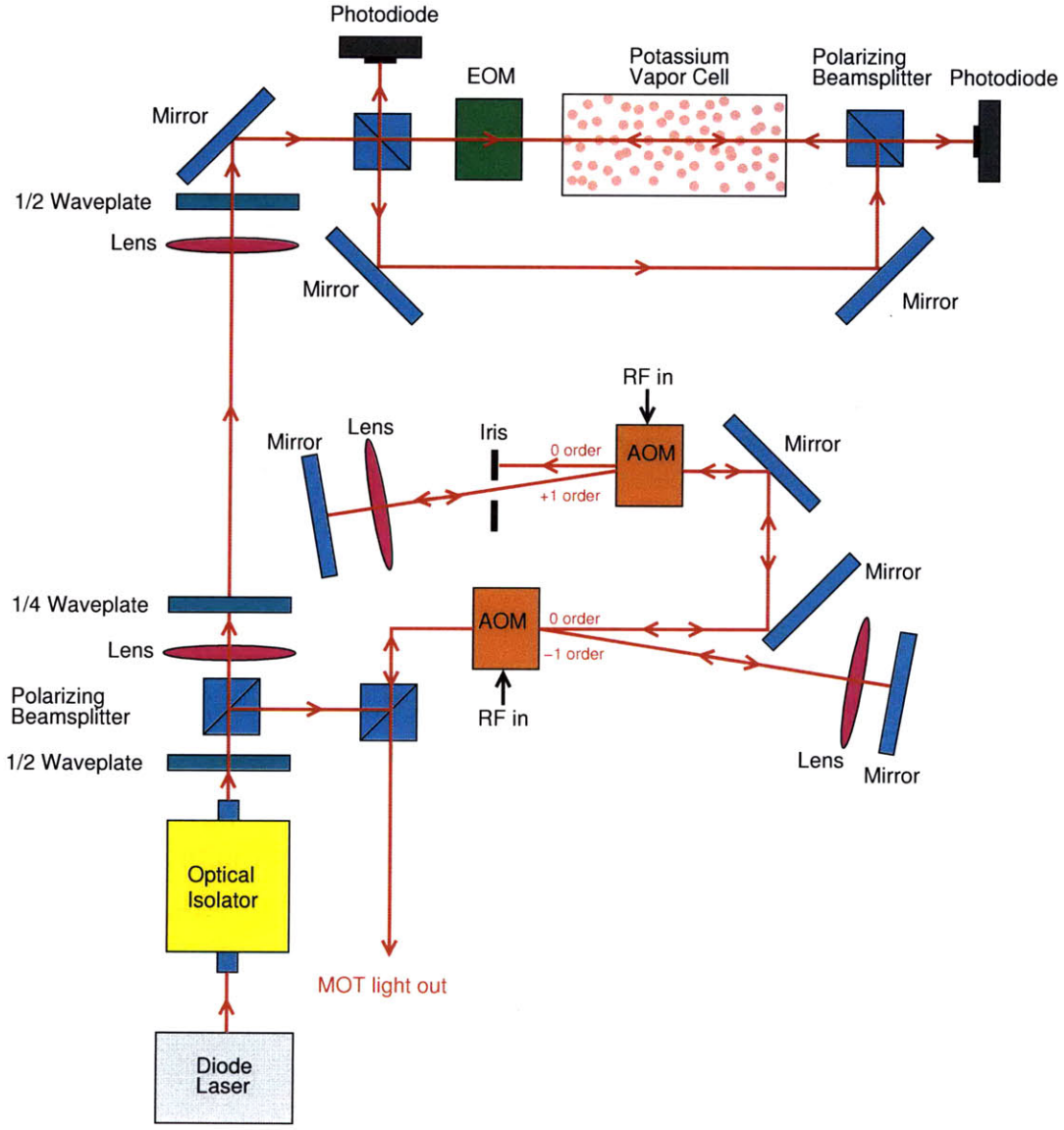

Figure 3-22: Potassium laser system.

Figure 3-23: The potassium cell, wrapped in tin foil, inside a metal tube, wrapped with a heating band. Windows are glued on two metal caps on the ends.

Figure 3-24: The cell is then wrapped in tin foil once more and placed inside the insulating PVC tube which is also attached to Thorlabs mounts.

First we wrapped the cell in tinfoil, put it in a metal tube, and secured it with plastic screws. Plastic screws are the best choice. They will not melt at these temperatures and they self-limit the amount of force that we apply to the cell. Metal screws are a bad idea, because it is easy to tighten them with a screwdriver until the glass cell breaks. (I did that.) We also put windows on the ends to keep the air around the ends of the cell hot. In previous attempts at a heater design, the windows were epoxied directly to the metal tube. However, it is likely that you will need to disassemble the enclosure multiple times, so in this design, we made two end caps by cutting and bending sheet metal and then we glued the windows to the caps. The caps are easy to remove. Then we wrapped the metal tube with a heating band, wrapped the whole enclosure in aluminum foil, and then put that in a PVC tube and secured it with plastic screws. Other designs used a metal outer enclosure, but I thought that plastic would give better insulation from the outside. Two Thorlabs posts are screwed into the bottom of the plastic enclosure. The potassium D1 line is shown in figure 3-25.

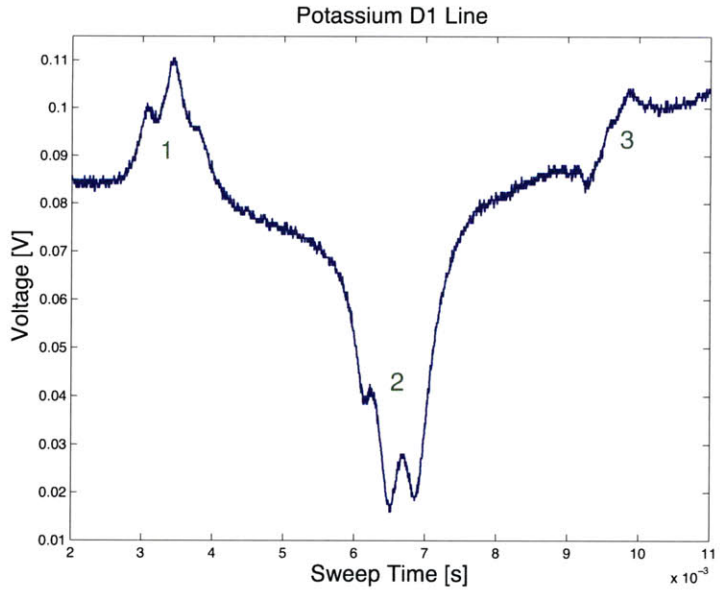

Figure 3-25: Potassium D1 line. 1 is the $2^2S_{1/2}, F = 2 \rightarrow 2^2P_{1/2}$ transition, 2 is the crossover resonance and 3 is the $2^2S_{1/2}, F = 1 \rightarrow 2^2P_{1/2}$ transition. The hyperfine structure in the $2^2P_{1/2}$ level is visible in each of the peaks. The middle, highest peak is the crossover, the smaller peak is the one that goes to the $2^2P_{1/2}, F = 1$ state, and the higher peak is the one that goes to the $2^2P_{1/2}, F = 2$ state.

We played with the laser power and the balance between the pump and probe beams (to, for example, reduce power broadening) in order to resolve the hyperfine energy splittings. The potassium D2 line and error signal are shown in figure 3-26.

3.8 Fabry-Perot Interferometer

3.8.1 Parallel Plane Mirror Cavity

A Fabry-Perot Interferometer consists of two parallel mirrors with high reflectivity and some small transmissivity. As shown in figure 3-27, the signal on the photodiode detector results from the laser beam entering the cavity and reflecting off the mirrors $2n$ times.The light interferes constructively when the round-trip path is an integer number of wavelengths $2L = n\lambda$, or $\nu = nc/2L$. The free spectral range is the

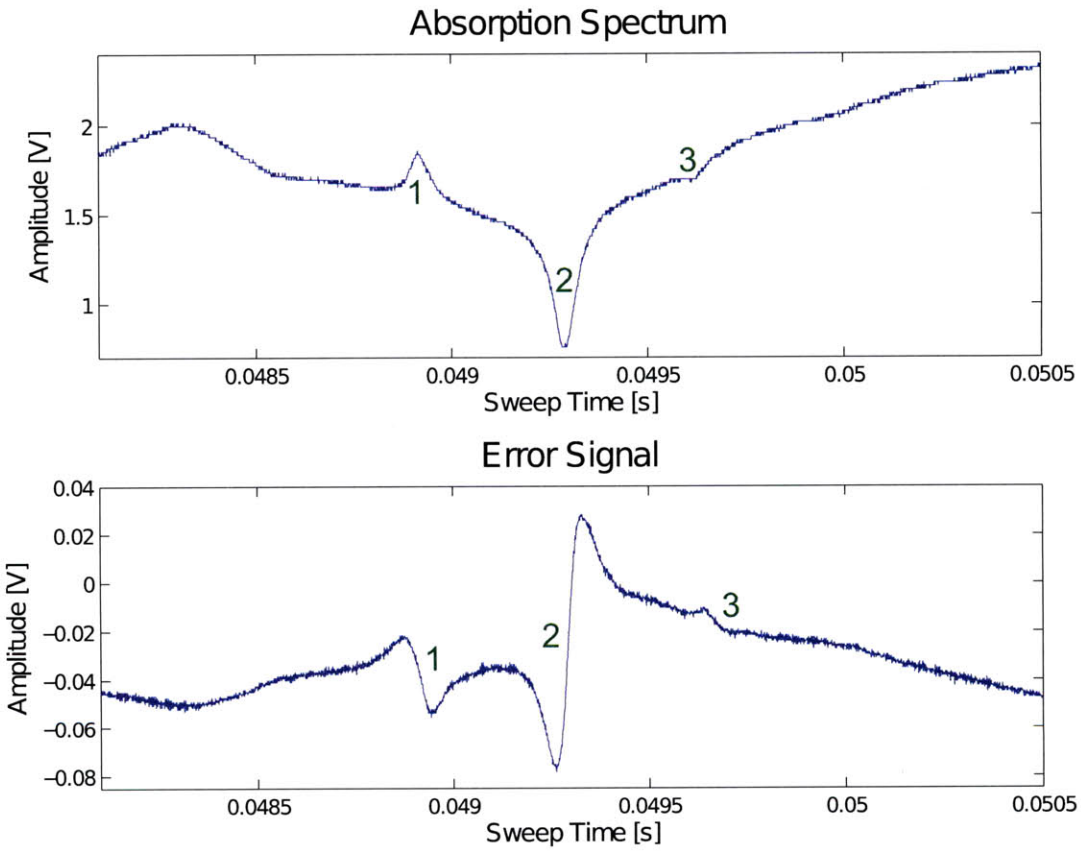

Figure 3-26: Potassium D2 line and error signal. 1 is the $2^2S_{1/2}, F = 2 \rightarrow 2^2P_{3/2}$ transition, 2 is the crossover resonance and 3 is the $2^2S_{1/2}, F = 1 \rightarrow 2^2P_{3/2}$ transition.

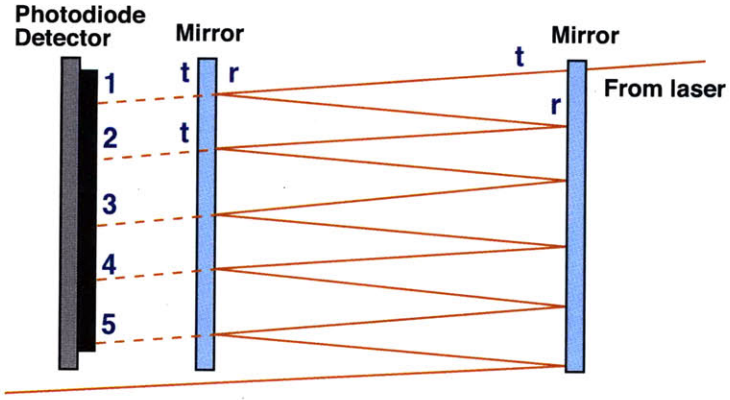

Figure 3-27: Illustration of light reflecting in a Fabry-Perot cavity.

wavelength separation between adjacent frequencies,

$$\Delta\nu_{\text{FSR}} = \frac{c}{2L} \tag{3.32}$$

Let t be the amplitude reflection, r be the amplitude transmission, $T = t^2$ be the power reflection and $R = r^2$ be the power transmission. Conservation of energy tells us that $R + T = 1$.[21] The round trip phase acquired by light of wavelength λ traveling between two mirrors with spacing L is,

$$\phi = \frac{2L}{\lambda}(2\pi) = \frac{2L\nu}{c}. \tag{3.33}$$

The total transmitted amplitude is the sum of the power of the light that is reflected $0, 2, 4, \ldots, 2n, \ldots$ times,

$$A_T = A_0 t^2 \sum_{n=1}^{\infty}(1 + r^{2n}e^{in2\phi}) = \frac{A_0 t^2}{1 - r^2 e^{i2\phi}} \tag{3.34}$$

and the transmitted intensity observed on the photodiode is,

$$I_T = \frac{1}{2}|A_T|^2 = \frac{I_0(1-R)^2}{(1-R)^2 + 4R\sin^2\phi} = \frac{I_0(1-R)^2}{(1-R)^2 + 4R\sin^2\frac{2\pi\nu ld}{c}}. \tag{3.35}$$

By setting $I_T(\phi) = \frac{1}{2}I_0$

The finesse F of the cavity is definited to be the ratio of the free spectral range and the full-width at half maximum of the peak.[1]

$$F \equiv \frac{\Delta\nu_{\text{FSR}}}{\Delta\nu_{\text{FWHM}}} = \frac{\frac{c}{2L}}{1} \tag{3.36}$$

3.8.2 Spherical-Mirror Mode-Degenerate Cavity

Mode-degenerate interferometers are advantageous for several reasons. They do not need to be mode-matched to the laser beam.[30] Interferometers which require mode-matching have extra transmission fringes due to the excitation of higher-order modes when they are not mode-matched properly. Because they do not need to be mode-matched, the interferometer does not need to be aligned on the axis of the interferometer. It is even a good idea to align the laser beam slightly off-axis so that the light from the interferometer does not travel back into the laser.[30]

A Fabry-Perot cavity with spherical mirrors of radius of curvature a supports Laguerre-Gaussian modes. The frequencies supported by the cavity are given by[30],

$$\nu = \frac{c}{2L}\left[q + \frac{1}{\pi}(1+m+n)\cos^{-1}\left(1-\frac{L}{a}\right)\right], \tag{3.37}$$

where m and n give the longitudinal mode orders and q gives the transverse mode order. If

$$\cos^{-1}\left(1-\frac{L}{a}\right) = \frac{\pi}{q}, \tag{3.38}$$

where l is an integer, the frequency dependence due to the transverse and longitudinal modes can be essentially combined and we have results very similar to the plane parallel mirror case. The peak frequencies are,

$$v = \frac{c}{2Ld}\left(n + (l+m+1)\frac{1}{q}\right) = \frac{c}{2qL}(qn + (l+m+1)). \tag{3.39}$$

By Bezout's lemma[4][31] 1 and q have greatest common divisor 1, so there exists n and $(l+m+1)$ such that $qn + (l+m+1) = 1$. Therefore, the free spectral range of

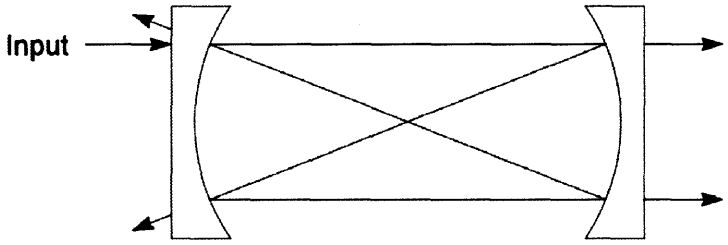

Figure 3-28: Classical optical path of a laser beam in a confocal Fabry-Perot cavity. Image from [1].

a cavity with degeneracy q is,

$$\delta\nu_{\mathrm{FSR,q}} = \frac{c}{2qL}. \tag{3.40}$$

The intensity profile is,

$$\frac{I_0(1-R)^2}{(1-R)^2 + 4R\sin^2\frac{2\pi\nu qL}{c}}, \tag{3.41}$$

the full width at half maximum is,

$$\Delta\nu_{\mathrm{FWHM}} = \frac{c(1-R)}{2\pi L}, \tag{3.42}$$

and the finesse is,

$$F = \frac{\pi}{q(1-R)} \tag{3.43}$$

In a confocal Fabry-Perot cavity, shown in figure 3-28, the focal points of the two spherical mirrors are at the same point. The focal length of a spherical mirror of radius of curvature a is $a/2$, so the cavity length $L = a$. Here, $L/a = 1$, so the degeneracy is,

$$q = \frac{\pi}{\cos^{-1}\left(1 - \frac{L}{R}\right)} = \frac{\pi}{\pi/2} = 2. \tag{3.44}$$

Therefore the free spectral range is,

$$\Delta\nu_{\mathrm{FSR,confocal}} = \frac{c}{4L}. \tag{3.45}$$

We could have expected this free spectral range intuitively because as shown in figure 3-28, the distance that a light beam travels before it overlaps with itself is $4L$, so the

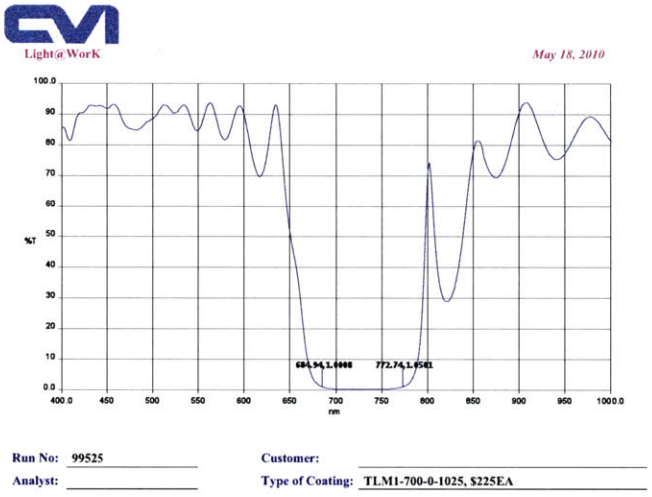

Figure 3-29: Transmission vs. wavelength data for the CVI Melles-Griot TLM1-700-0 tunable laser line mirror. The $\approx 1\%$ transmission at both 671 nm and 767 nm makes this a good mirror for potassium and lithium Fabry-Perot cavities.

effective optical path length is $4L$. In addition, the intensity profile is,

$$\frac{I_0(1-R)^2}{(1-R)^2 + 4R\sin^2\frac{4\pi\nu L}{c}}, \tag{3.46}$$

the full width at half maximum is,

$$\Delta\nu_{\text{FWHM}} = \frac{c(1-R)}{2\pi L} = \frac{\Delta\nu_{\text{FSR}}}{F}, \tag{3.47}$$

and the finesse is,

$$F = \frac{\pi}{2(1-R)}. \tag{3.48}$$

3.8.3 PZT Driver

We use a homemade high-voltage amplifier to provide enough voltage on the PZT to sweep the cavity length. The schematic for the amplifier is shown in figure 3-30 and was provided to us by the Vuletic group. The input signal first travels through IC1 (INA114P), a high input impedance buffer that eliminates ground loops. The

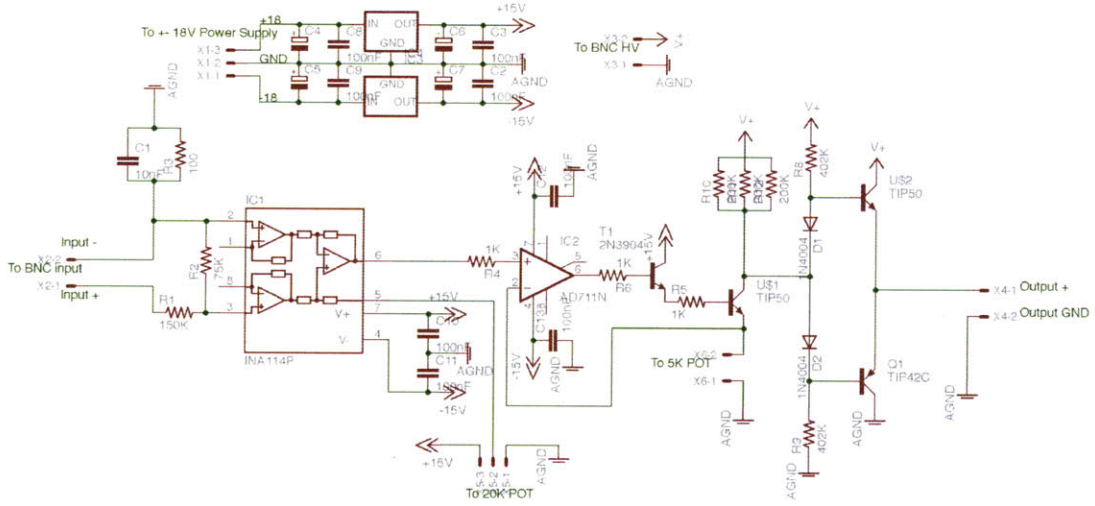

Figure 3-30: Schematic of the high-voltage amplifier that drives the PZT.

signal then passes through a two-stage amplifier, composed of T1 (2N3904) and the high-voltage U$1 (TIP50). The amplifier is controlled by feedback from the op-amp IC2, which can also add an offset through the inverting input. In the final stage, the signal passes between two transistors U$2 (TIP50) and Q1 (TIP42C) in a push-pull configuration. A PNP transistor can only source current and a NPN transistor can only sink current. So when we want to drive both positive and negative current loads, we use the two together. Also the two diodes D1 (N4004) and D2 (N4004) help to eliminate crossover distortion[18] caused by the $\approx$ .6V forward voltage drop from the emitter to the base on a PNP transistor and from the base to the emitter on an NPN transistor. The diodes give the PNP base a signal that is $\approx$ .6V lower and give the NPN base a signal that is $\approx$ .6V higher than the original. On the power rails, different capacitors run between V_+, V_- and ground to filter out high-frequency noise. The gain, amplitude and offset of the signal are all controlled by connectors that run to potentiometers.

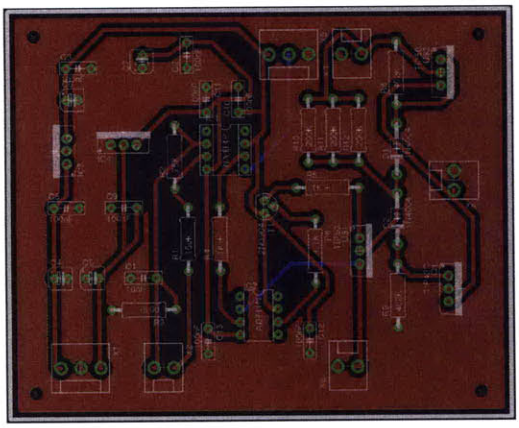

Figure 3-31: PCB design for the high-voltage amplifier that drives the PZT.

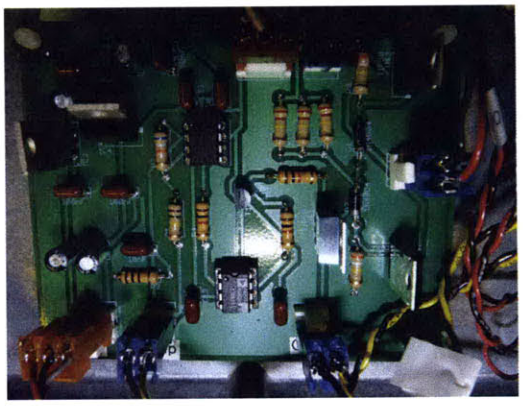

Figure 3-32: Populated PCB. The parts follow the silkscreen except the TIP42c is reversed.

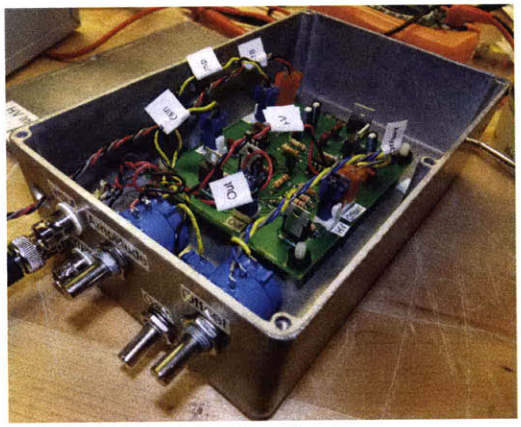

Figure 3-33: Inside the PZT driver box.

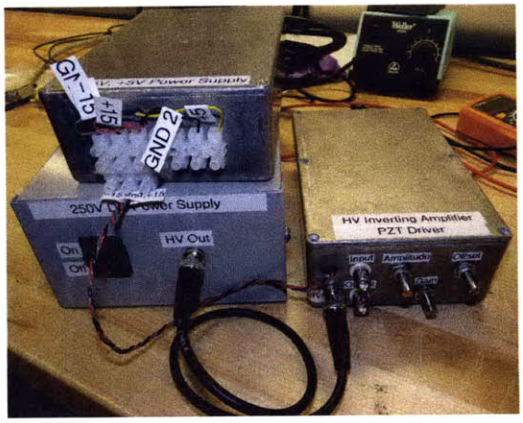

Figure 3-34: The PZT driver setup with a ±15V and 250V power supplies and the PZT driver box.

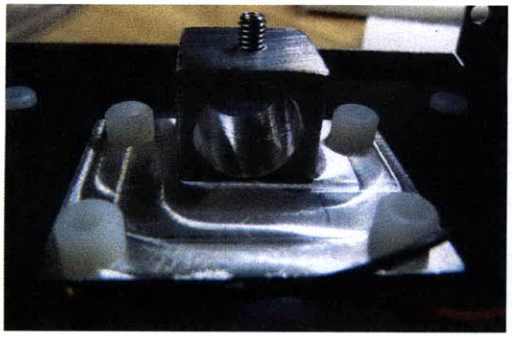

Figure 3-35: Lens tube housing, milled to cover the TEC.

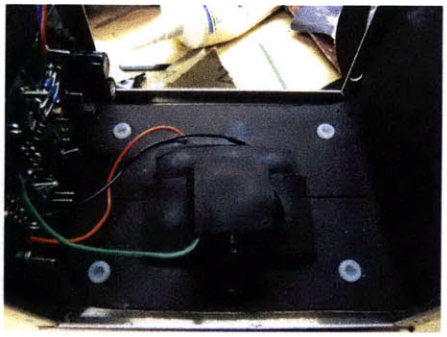

Figure 3-36: Complete assembled slave laser.

3.9 New Homemade Slave Laser

The design for a homemade slave laser housing is shown in figures 3-35 and 3-36. The lens tube housing shown in figure 3-35 was designed to have the minimum possible thermal mass and also do cover the whole TEC for efficient heat transfer. The diode and the TEC attach to the same PCB used for the master lasers and can connect to commercial or homemade temperature and current controllers.

3.10 Laser Design Evolution

The two newest lasers are shown in figures 3-37 and 3-38. We used a new, sturdier aluminum box. We put the laser on the box lid and used the rest of the box as the laser cover. This is nice because it allows access all around the laser mount. In the previous design, you had to really pull on the cover to get it off, which could sometimes misalign the laser. In this design, you can simply lift the top off. In general, you should never have wires or connectors going through the part of the box that you remove. Therefore, inspired by Shin Inouye's lasers, we ran the serial cable and BNC connectors through the bottom of the box. This worked out well for the lithium laser, as we mounted it on the usual rubber posts as shown in figure 3-37. However, for the higher power sodium laser, we wanted very good heat sinking, so we milled slots in the side of the aluminum block and mounted the block directly to the

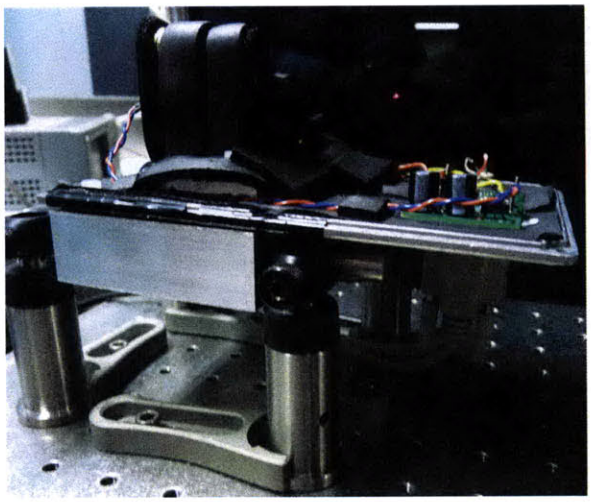

Figure 3-37: Lithium laser. The two serial cables and the BNC cable to drive the PZT all to through the bottom of the box.

optical table as shown in 3-38. Then there was not enough space for a regular serial cable. But we made our own cable that did fit by cutting off the end of a serial cable, soldering the wires to a serial connector and wrapping everything in tin foil. In the future, we should switch to having two right-angle DB-9 serial cable connectors on the PCB.

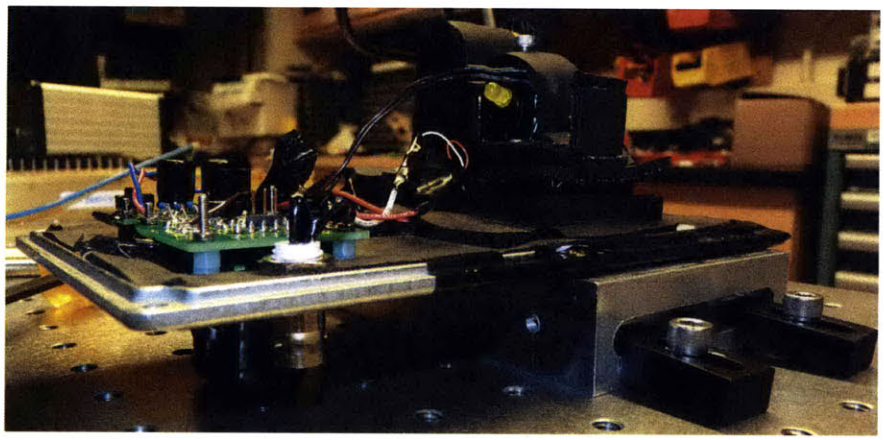

Figure 3-38: 1178 nm diode laser housing for sodium. We put the aluminum block directly on the optical table for better heat sinking.

Chapter 4

Vacuum System

4.1 Design and Setup

Figure 4-1 shows the entire vacuum system. Lithium from the oven will travel through a nozzle and a differential pumping tube, down the Zeeman slower and to the science chamber where it will be trapped in a 3D MOT. Our enriched potassium-40 sample will be warmed slightly and enter the glass cell where the 2D MOT will be.

4.1.1 Glass Cell

The design for the glass cell is shown in figure 4-2 and pictures of the real glass cell are shown in figures 4-3, 4-4 and 4-5. We load our transversely-cooled potassium into the 3D MOT by using a push beam, which is a set of counterpropagating lasers that are detuned from each other in the lab frame, but look like optical molasses in a frame that moves at some velocity v. The copper mirror is to reflect the push beam into the hole that the atomic beam will pass through. We use the glass cell because enriched potassium-40 is very expensive so we would like to recover any of it that sticks to our chamber. Similarly, we use the large copper mirror to block any potassium that does not make it through the hole in the center, so we can simply heat the copper to recover the potassium.

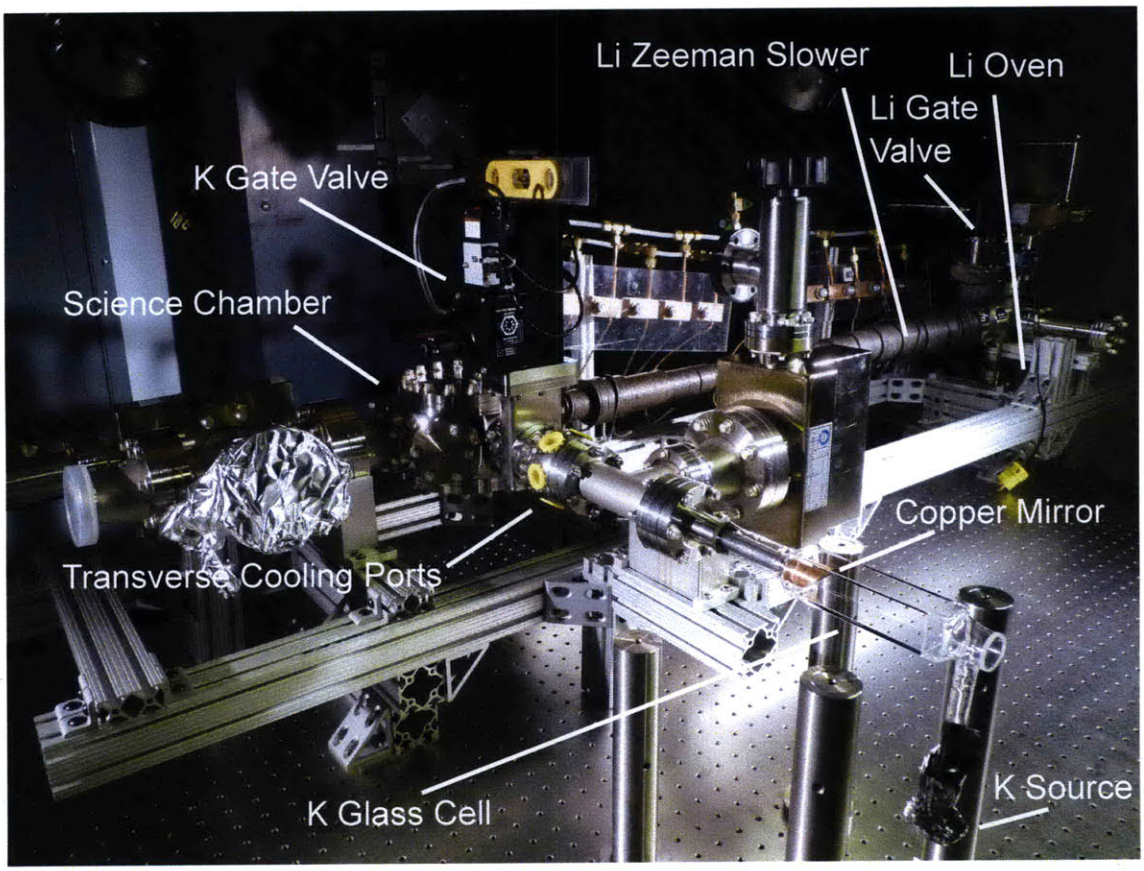

Figure 4-1: The entire vacuum system, which we disassembled, cleaned, reassembled and supported with 80-20.

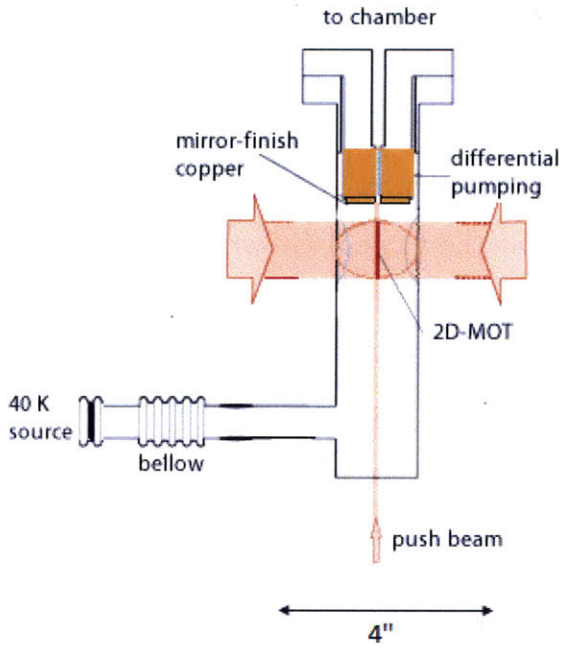

Figure 4-2: Glass cell design with 2D MOT. Figure modified by Ibon Santiago from [32].

Figure 4-3: Side view.

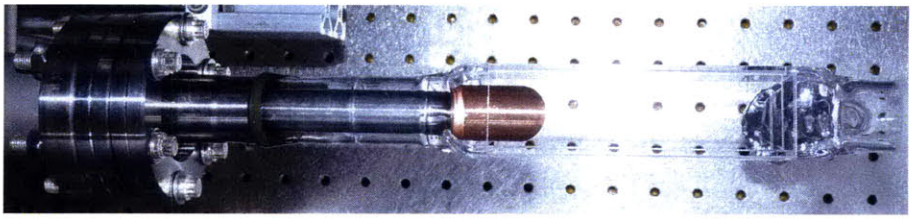

Figure 4-4: Top view.

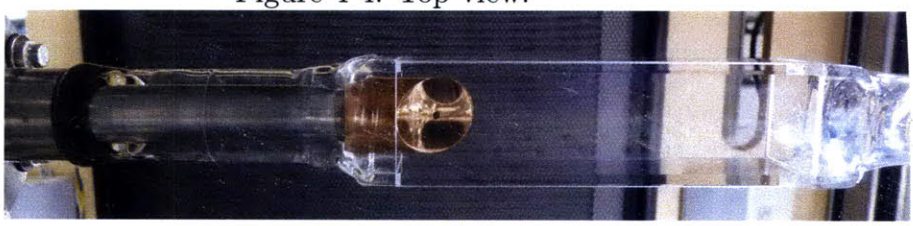

Figure 4-5: Bottom view, with a good view of the mirror-polished copper to reflect the push beam and the hole that the atoms travel through.

4.1.2 Polishing to a Mirror Finish

First we used the finest sandpaper in the Edgerton shop to get rid of tool marks and make the surface flat. Then, we used the South Bay Technology 920 Lapping and Polishing Machine at the Crystal Growth Shared Experimental Facility in the Center for Materials Science and Engineering on the 3rd floor of building 13. The lapping paper has an adhesive backing and you take it off and stick it to the wheel of the polishing machine. The wheel spins and you let water slowly drip over the paper for lubrication. We used a series of ever-finer lapping paper: 20, 12, 9, and 3 microns. Each time we went to finer lapping paper, the mirror surface looked less cloudy and the scratches looked finer. However, when we went below 3 microns, to 1, .3 or .1 microns, the scratches looked much worse. After many attempts and talking to the research scientists there, we decided that because the finer paper is thinner, the surface is more susceptible to being scratched by imperfections on the wheel. So after 3 microns, we switched to using polishing cloth, which was thicker than the lapping paper and .1 micron polishing powder. We mixed the polishing powder with the dripping water and held the surface on the cloth as the wheel spun. The results were quite good: by eye, an incident and reflected laser beam looked the same. We measured the reflectivity of the copper mirror after it was in the glass cell. The laser input was 16 mW and the output was 12 mW.

$n_{\text{glass}} \approx 1.5$ and $n_{\text{air}} \approx 1.0$. The amount of light transmitted and reflected when moving between media of different refractive indices is given by the Frensel equations. When the light is incident to the plane of the interface, the equations are easy,

$$R = \left(\frac{n_1 - n_2}{n_1 + n_2}\right)^2 \approx \left(\frac{1.5 - 1.0}{1.5 + 1.0}\right)^2 = 4\% \tag{4.1}$$

Therefore the reflectivity of our copper mirror is,

$$\frac{12}{16} \cdot \left(\frac{1}{.96}\right)^4 \approx 88\%. \tag{4.2}$$

4.1.3 Cleaning for Ultra-High Vacuum

We used the following order to clean our parts for UHV:

1. Warm deionized water and detergent, 30 minutes
2. Cold deionized water, 30 minutes
3. Cold acetone, 30 minutes
4. Cold methanol, 30 minutes

Acetone is good at dissolving heavy organic materials [17], but it leaves a residue. Methanol can remove the acetone residue and does not leave its own residue.

4.1.4 Atomic Beam Shutter

The atomic beam shutter is a flag on a post, screwed into a blank, which is attached to a flexible bellow and then an actuator. By moving the actuator back and forth we control whether the flag is blocking the atomic beam or not. The parts of an atomic beam shutter and relevant dimensions are shown in figures 4-6, 4-7, 4-8, and 4-9. We want to drill and tap in the stainless steel blank without destroying the integrity of the vacuum. Instead of drilling and tapping for 1/4-20 (which was the outer diameter of the original rod), we drilled 1/4" deep for 8-32. Then we turned down the end of the rod to .1640" major diameter for 8-32 threads and threaded it using a die. Because the die is tapered, we had to cut thread reliefs at the top down to the .1248" minor diameter for 8-32 threads. In addition, any screws in a vacuum system can cause virtual leaks - pockets of air that slowly leak into the chamber and take a long time to be pumped out. To eliminate virtual leaks, we mounted a slit saw on a mill and cut a small slit to allow pockets of air to escape.

4.2 Titanium-Zirconium-Vanadium Coating

I have not failed. I've just found 10,000 ways that won't work.

-Thomas Edison

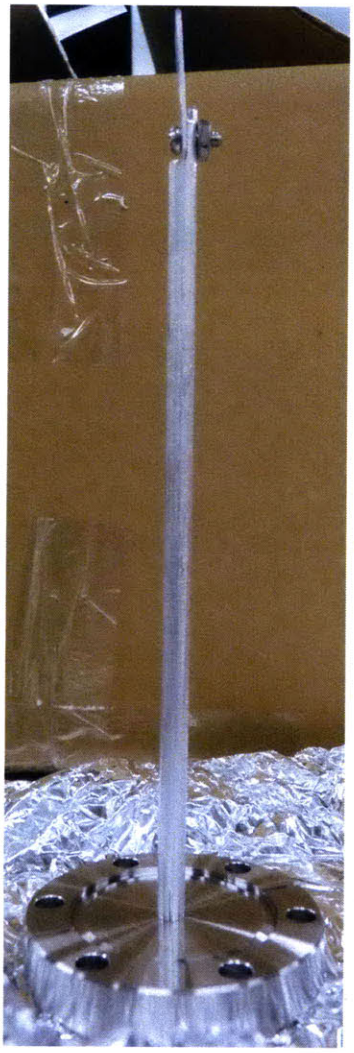

Figure 4-6: Atomic beam shutter with the rod screwed into a 1/4" deep 8-32 tapped hole in a $2\frac{3}{4}$" blank.

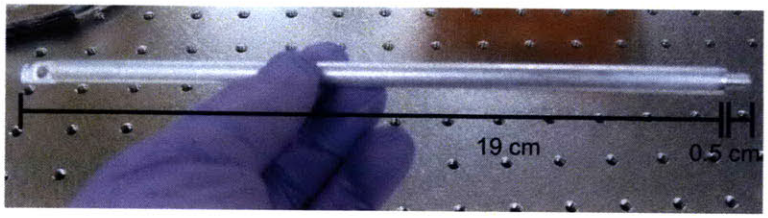

Figure 4-7: Shutter length dimensions.

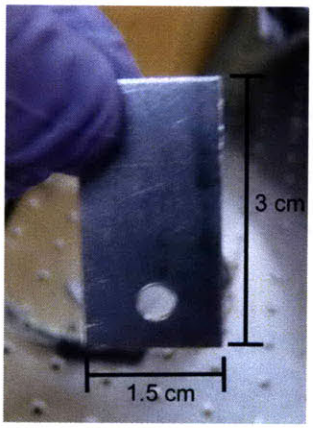

Figure 4-8: Shutter flag dimensions.

Figure 4-9: The end was turned down to .1640" major diameter for 8-32 threads, .1248" minor diameter thread relief was cut at the top of the threads, and a slit was cut to eliminate virtual leaks.

Figure 4-10: The original Ti-Zr-V feedthrough, with the filaments wrapped around ceramic rods and attached to the power line at the base and ground at the top.

I wrote this section with the help of Ibon Santiago, one of my partners in the coating endeavor. One of the technical challenges in cold atoms experiments consists in obtaining good vacuum. Normally a MOT requires at least 10^{-6}Torr, however, further cooling or quantum degenerate regimes cannot be obtained without UHV (10^{-9} to10^{-13} Torr). Non-evaporative getter coating of a vacuum chamber allows pumping once the chamber is closed and baked at a certain temperature. An alloy of Ti-Zr-V at a particular ratio and thickness provides a reactivation temperature as low as 200^{o}C[8]. When the alloy reactivates, it expels all of the particles it has "gotten", we pump them out, and it is then ready to be a getter again. We are currently studying how to deposit each element at a controlled rate.

Our coating method is to perform thermal evaporation of filaments of each element. If the filaments are fired simultaneously, an alloy will form on the walls of the vacuum chamber. The filaments are held by copper lugs attached to an electric feedthrough that goes into the vacuum. Electrical contacts are made in an aluminum block, as shown in our original scheme in figure 4-10. Particles are expected to stick to the stainless steel wall immediately after evaporation. The motion is ballistic if the mean free path is larger than the size of the chamber. At a pressure of 10^{-6} Torr we calculated that a particle would have to travel about 165 feet to collide with other particles. To obtain this pressure we pump down the chamber with a roughing pump and then a turbo pump. Once the chamber is in the desired pressure, evaporation occurs at a controlled current.

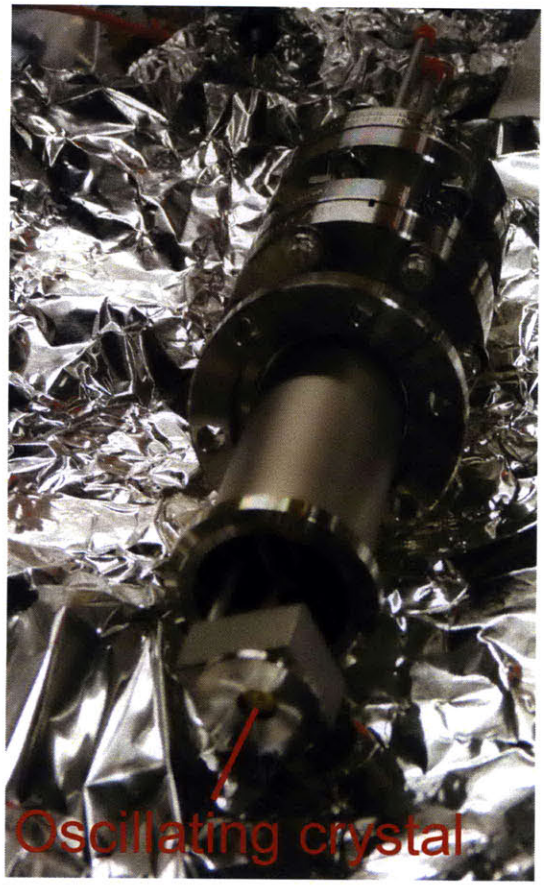

Figure 4-11: The oscillating crystal sensor that we use to measure the deposited film thickness.

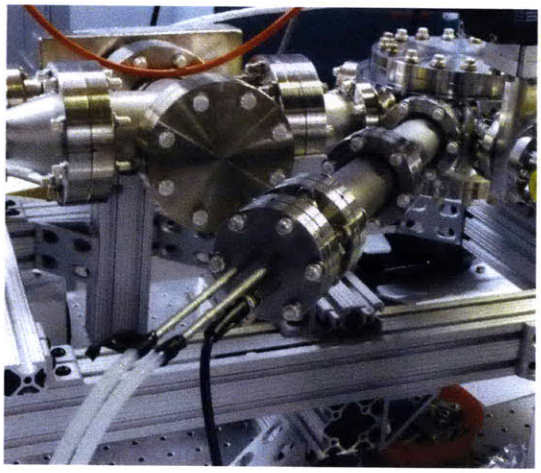

Figure 4-12: The sensor shown from the other side, with water cooling attachments.

A quartz crystal oscillator, shown in figures 4-11 and 4-12, attached to a water-cooled sensor has been placed inside the chamber. Changes in oscillation frequency of the oscillator can be directly related to the mass deposition rate. This method allows direct control on the desired deposition rate depending on the selected current in the power supply.

Filaments tend to break if too much current is run through them for a long time. Sagging of filaments and melting have been constant problems that have been overcome by selecting thicker wires and by looping the filament around a ceramic rod. Zirconium presents a special difficulty due to its different vapor pressure and thermal properties as compared to Ti and V. Its melting temperature 1855°C is very close to the temperature at which reasonable sublimation occurs (1700°C). This is why

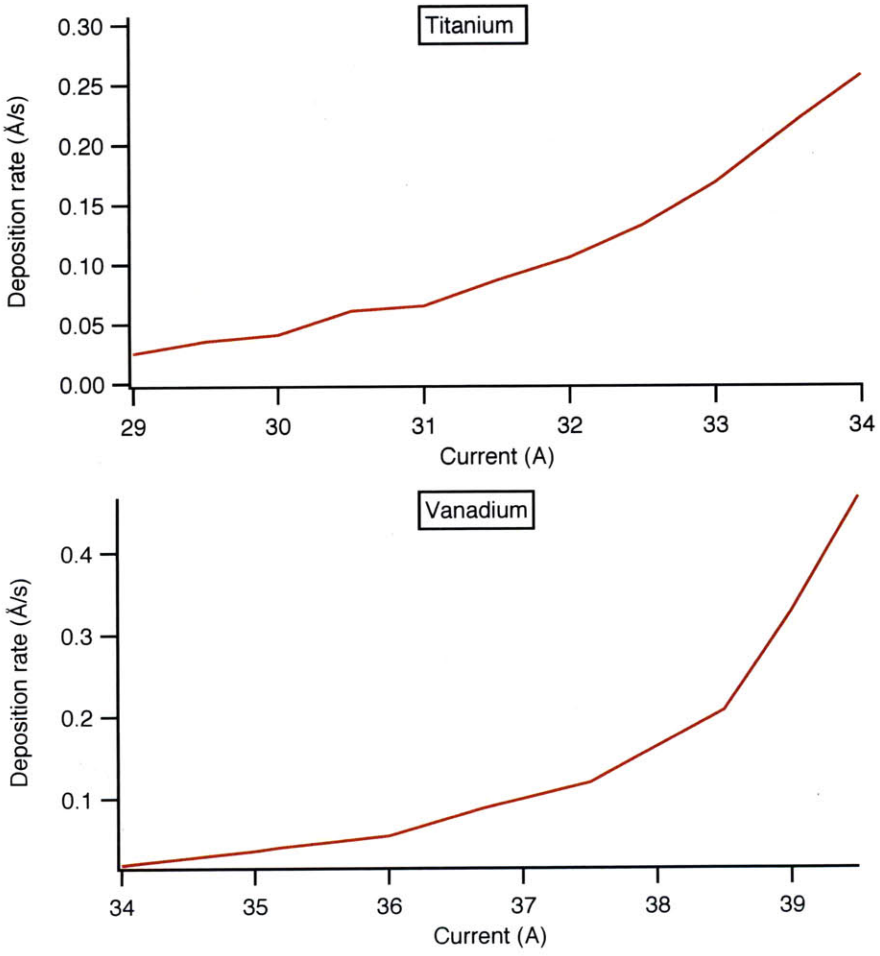

Figure 4-13: Deposition rate vs. current for titanium and vanadium. Both curves follow rate $\propto$ (current)^2 as expected. Figures created by Ibon Santiago.

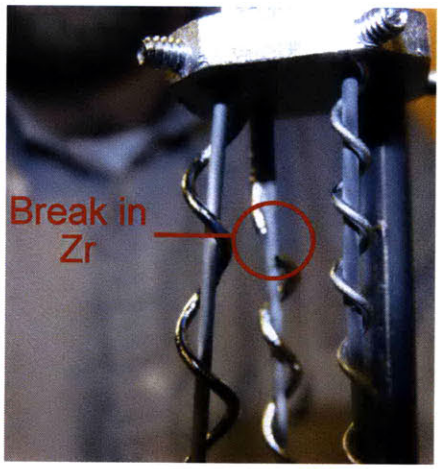

Figure 4-14: Break in the Zr filament.

evaporation often terminates abruptly when the filament melts and breaks. When we tried to run current through a 1 mm diameter piece, it consistently broke, as shown in figure 4-14. In addition to our traditional 1 mm pieces, we tried a thicker 2 mm piece and also tried heating Zr via a tungsten filament. We put the feedthrough in with 3 different Zr coating methods to see which was the best, as shown in figure4-15. $P = I^2R$ where P is the power being dissipated in the filament, I is the current going through filament , and R is the resistance of the filament. The resistance $R \propto 1/\sigma$ where $\sigma \propto 1/d^2$ is the cross-sectional area and d is the diameter. So when we double d we need to also double I to dissipate the same power in the filament. The larger filament also has more thermal mass, but on the other hand, it has a smaller surface area to volume ratio, so it radiates less of its total thermal energy. When we supported it with ceramic, it did not break. Figure 4-16 shows some Zr actively being fired at 115 amps, which was about the limit of the power supply. Even at currents that high, we did not observe significant deposition.

Further complicating the Zr issues, at first we measured the mass using a gold-plated crystal, which was not the correct crystal plating for zirconium. When we fire Zr on gold, something called high-stress metallizing can occur. According to [34], thin films of Zr, Ti and other metals can develop high stresses when deposited. At thicknesses higher than 1000 $\AA$, the films can crack or flake and even crack the

Figure 4-15: Feedthrough with three different attempts to sublimate Zr From left to right: Heating by running current through a 1 mm diameter rod, heating by running current through a 2 mm diameter rod, and heating wrapping a 1 mm diameter rod around a tungsten filament and running current through tungsten.

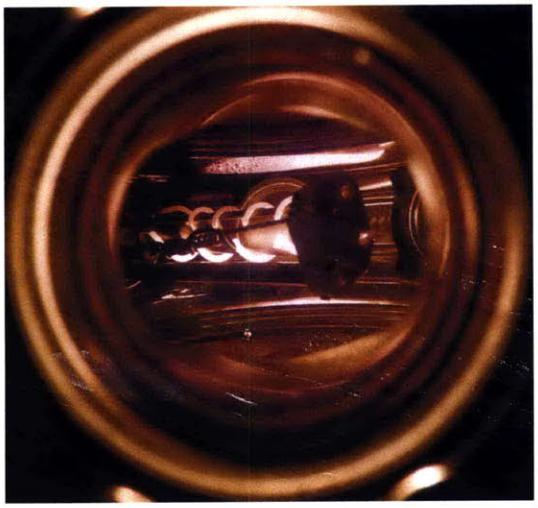

Figure 4-16: The 2 mm diameter rod with 115 amps running through it. The whole feedthrough becomes so hot that the 1 mm diameter rod starts to glow too.

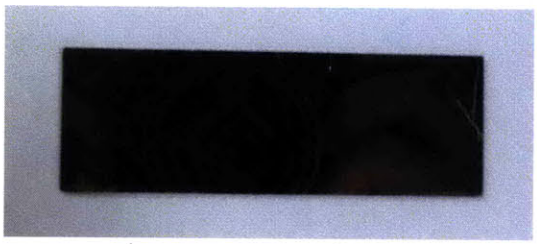

Figure 4-17: The coated microscope slide we used when we were not sure if the sensor was working properly. In this picture, the slide is sitting on a piece of white paper, so we can see it is very well coated.

substrate they are coated onto. These stresses are transmitted to the crystal itself and causes the sensor to show either sudden rate jumps or rapidly occurring positive and negative rate spikes[34]. The manufacturer recommends using a silver-coated crystal instead of the gold one we were using[34]. We consistently measured zero deposition rates for many trials, and we put a glass slide in the chamber to see if maybe coating was happening but the sensor had a problem. As shown in figure 4-17, the slide came out very well coated, so we knew there was a problem with the sensor. Then we ordered some silver-coated crystals and saw positive deposition rates.

Once we figured out what was wrong with the crystal, we found that the technique with the tungsten as an external heating source (or crucible), worked quite well. We selected Tungsten because of its high melting temperature (3000^{o}C) and negligible vapor pressure. By looping zirconium around a tungsten filament, successful deposition of zirconium has been achieved, as shown in figure 4-18. Due to its known properties as a getter, while evaporating a difference in two orders of magnitude has been observed in the pressure reading of the chamber (from 10^{-5} Torr down to 10^{-7} Torr).

We used the filament heating source method outlined in [9]. Using a different heating source other than the zirconium itself is a good idea, because we might have to melt some of the zirconium in order to get reasonable evaporation rates. A commercially-available helical filament source like tungsten made with multistrand wire for larger surface area is commonly used.[9] The goal here is to actually melt *all* of the evaporant, coat the source, bring the temperature back down, and then evaporate

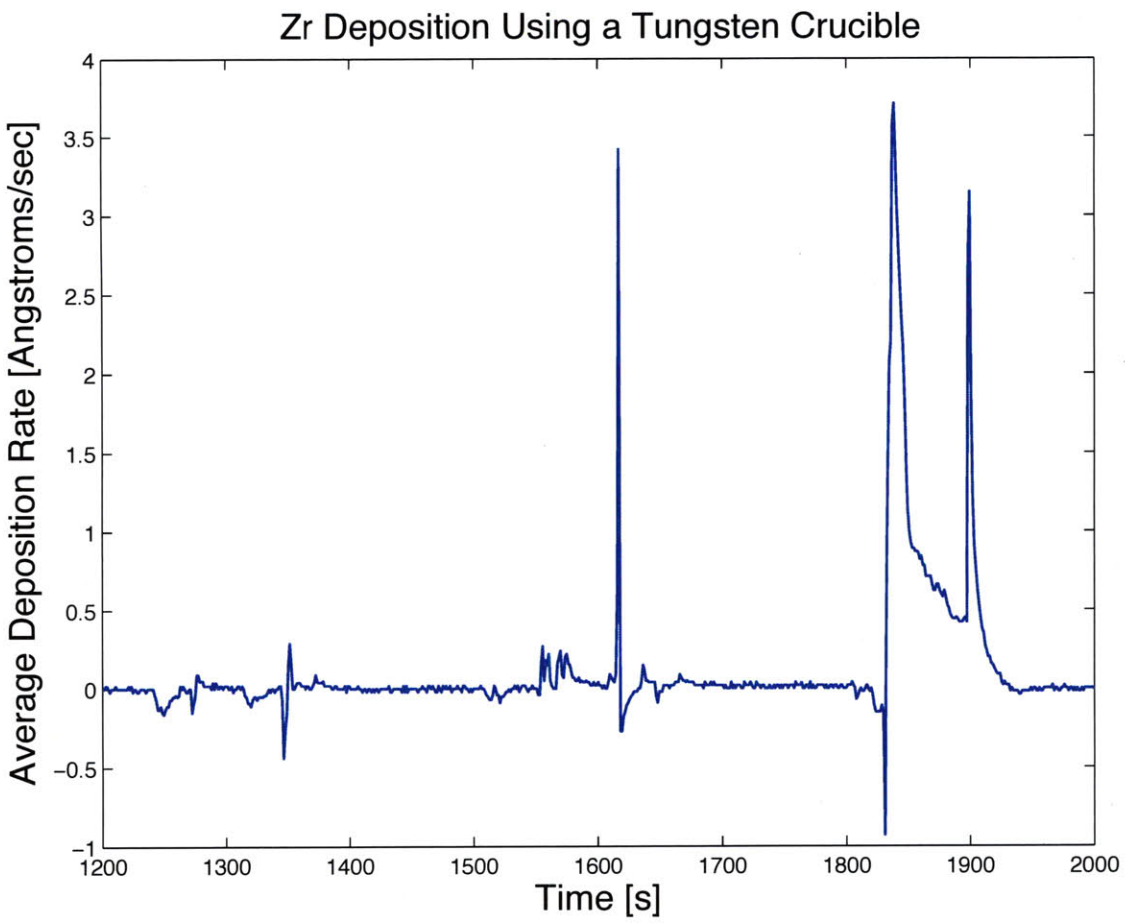

Figure 4-18: The final setup where we did get a positive deposition rate of zirconium. The large spikes indicate different parts of the zirconium melting and making contact with the tungsten.

at a controlled rate. Vapor emission from a helical source is multidirectional, so this is better than some other methods like using a boat.

Figure 4-18 shows our current results for evaporation of zirconium off of a tungsten filament. We have achieved positive deposition rates, which is good progress, but we have not managed to evaporate at a controlled rate yet. The large spikes happen when different parts of the zirconium melt and make contact with the tungsten. The overall rate declines and drops to zero when we heat and strain the tungsten so much that it actually breaks. Our next goal will be to melt the zirconium uniformly without breaking the tungsten so that we can then bring the temperature down and evaporate.

Chapter 5

Conclusion and Future Work

In conclusion, we have successfully set up the potassium and lithium laser systems, assembled the vacuum system, and we are coming close to the correct method for coating our vacuum system. The next step will be to build lithium and potassium Fabry-Perot cavities to check the frequency outputs of the two double-pass AOMS, then build tapered amplifiers to amplify the lithium and potassium light.

5.1 Suggested Improvements to Apparatus

We could implement a simple voltage clamp like the one shown in figure 5-1 to protect our PZTs against negative voltage. Also the lockbox and PZT driver require an external sawtooth signal from a function generator, which we could also get using a simple 555 timer IC. Another idea is that, to help stay on the same laser mode when we scan, we could feed forward the PZT scanning signal to the current controller.

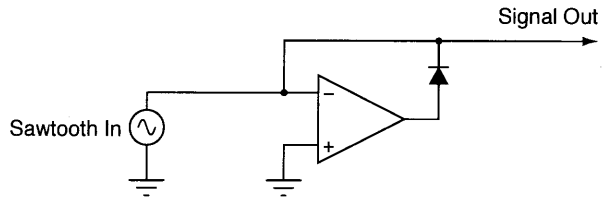

Figure 5-1: Circuit that can protect the PZT from negative voltage.

Bibliography

[1] Expt. 71 - fabry-perot cavities and fm spectroscopy. Ph 77 Advanced Physics Laboratory - Atomic and Optical Physics.

[2] The nobel prize in physics 1997, 1997. Nobel Prize Website, accessed 5/21/2010.

[3] L. Allen and J. H. Eberly. *Optical Resonance and Two-Level Atoms.* Dover Publications Inc., 1975.

[4] Titu Andreescu, Dorin Andrica, and Zuming Feng. *104 Number Theory Problems.* Birkhäuser, 2007.

[5] S. V. Andreev, V. I. Balykin, V. V. Letokhov, and V. G. Minogin. Radiative slowing and reduction of the energy spread of a beam of sodium atoms to 1.5 k in an oppositely directed laser beam. *JETP Lett*, 34(8), 1981.

[6] E Arimondo, M. Inguscio, and P. Violino. Experimental determinations of the hyperfine structure in the alkali atoms. *Rev. Mod. Phys.*, 49:31–75, 1977.

[7] George Bekefi and Alan Barrett. *Electromagnetic Vibrations, Waves, and Radiaton.* The MIT Press, 1977.

[8] C. Benvenuti. Non-evaporable getters: From pumping strips to thin film coatings. Technical report, CERN, 2001.

[9] Robert Berry, Peter Hall, and Murray Harris. *Thin Film Technology.* D. Van Nostrand Company, 1968.

[10] Gary C. Bjorklund. Frequency-modulation spectroscopy: a new method for measuring weak absorptions and dispersions. *Optics Letters*, 5:15–17, January 1980.

[11] Ananth P. Chikkatur. *Colliding and Moving Bose-Einstein Condensates: Studies of Superfluidity and optical tweezers for condensate transport.* PhD thesis, Massachusetts Institute of Technology, October 2002.

[12] E. A. Donley, T. P. Heavner, F. Levi, M. O. Tataw, and S. R. Jefferts. Double-pass acousto-optic modulator system. *Review of Scientific Instruments*, 76(063112), 2005.

[13] W. Ertmer, R. Blatt, J. L. Hall, and M. Zhu. Laser manipulation of atomic beam velocities: Demonstration of stopped atoms and velocity reversal. *Physical Review Letters*, 54(10), 1985.

[14] L. Ricci et. al. A compact grating-stabilized diode laser system for atomic physics. *Optics Communications*, 117:541–549, June 1995.

[15] Kenneth J. Günter. Design and implementation of a zeeman slower for ^{87}rb, March 2004.

[16] C. J. Hawthorn, K. P. Weber, and R. E. Scholten. Littrow configuration tunable external cavity diode laser with fixed direction output beam. *Review of Scientific Instruments*, 72(12), 2001.

[17] Yun He, Yulin Li, Nariman Mistry, and Shlomo Greenwald. Cornell electron storage ring phase-iii interaction region vacuum chamber. *Journal of Vacuum Science and Technology*, 19:1699–1703, December 2000.

[18] Paul Howoritz and Winfield Hill. *The Art of Electronics.* Cambridge University Press, second edition, 2001.

[19] Wolfgang Ketterle and Isaac Chuang. 8.422 class notes. Spring 2009.

[20] Zhong Lin, Kazuko Shimizu, Mingsheng Zhan, Fujio Shimizu, and Hiroshi Takuma. Laser cooling and trapping of li. *Japanese Journal of Applied Physics*, 30(7B):1324–1326, 1991.

[21] A. Melissinos. *Experiments in Modern Physics.* Academic Press, Burlington, 2003.

[22] Harold J. Metcalf and Peter van der Straten. *Laser Cooling and Trapping.* Springer, 1999.

[23] Todd P. Meyrath. Electromagnet design basics for cold atom experiments, August 2004.

[24] W. Müller and W. Meyer. Ground-state properties of alkali dimers and their cations (including the elements li, na, and k) from ab initio calculations with effective core polarization potentials. *J. Chem. Phys.*, 80(3311), 1984.

[25] K.-K. Ni, S. Ospelkaus D. Wang, M.H.G. de Miranda, , A. Pe'er, B. Neyenhuis, J. J. Zirbel, S. Kotochigova, P.S. Julienne, D. S. Jin, and J. Ye. A high phase-space-density gas of polar molecules. *Science*, 322(231), October 2008.

[26] S. Ospelkaus, K.-K. Ni, G. Quemener, B. Neyenhuis, D. Wang, M.H.G. de Miranda, J. L. Bohn, J. Ye, , and D. S. Jin. Controlling the hyperfine state of rovibronic ground-state polar molecules. *Physical Review Letters*, 104(030402), 2010.

[27] S. Ospelkaus, K.-K. Ni, D. Wang, M.H.G. de Miranda, B. Neyenhuis, G. Quemener, P.S. Julienne, J. L. Bohn, D. S. Jin, and J. Ye. Quantum-state controlled chemical reactions of ultracold potassium-rubidium molecules. *Science*, 327, February 2010.

[28] William D. Phillips. Laser cooling and trapping of neutral atoms. In E. Arimondo, W. D. Phillips, and F. Strumia, editors, *Proceedings of the International School of Physics "Enrico Fermi"*, 1992.

[29] F. Reif. *Statistical Physics.* McGraw-Hill, 1967.

[30] Douglas Sinclair. Scanning spherical-mirror interferometers for the analysis of laser mode structure. Technical report, Spectra-Physics, Incorporated, 1968.

[31] Ariel Sommer. Fabry-perot, November 2008. Zwierlein group meeting presentation.

[32] Tobias Tiecke. *Feshbach resonances in ultracold mixtures of the fermionic quantum gases.* PhD thesis, University of Amsterdam, 2009.

[33] Cheng-Hsun Wu. How to lock a laser, February 2009. Zwierlein group meeting presentation.

[34] X-TRONIX. *Selecting the Best Crystal for Your Coating Process*, 2010.

[35] Martin Zwierlein. Cooling and trapping a bose-fermi mixture of dilute atomic gases. Undergraduate Thesis, 2001.